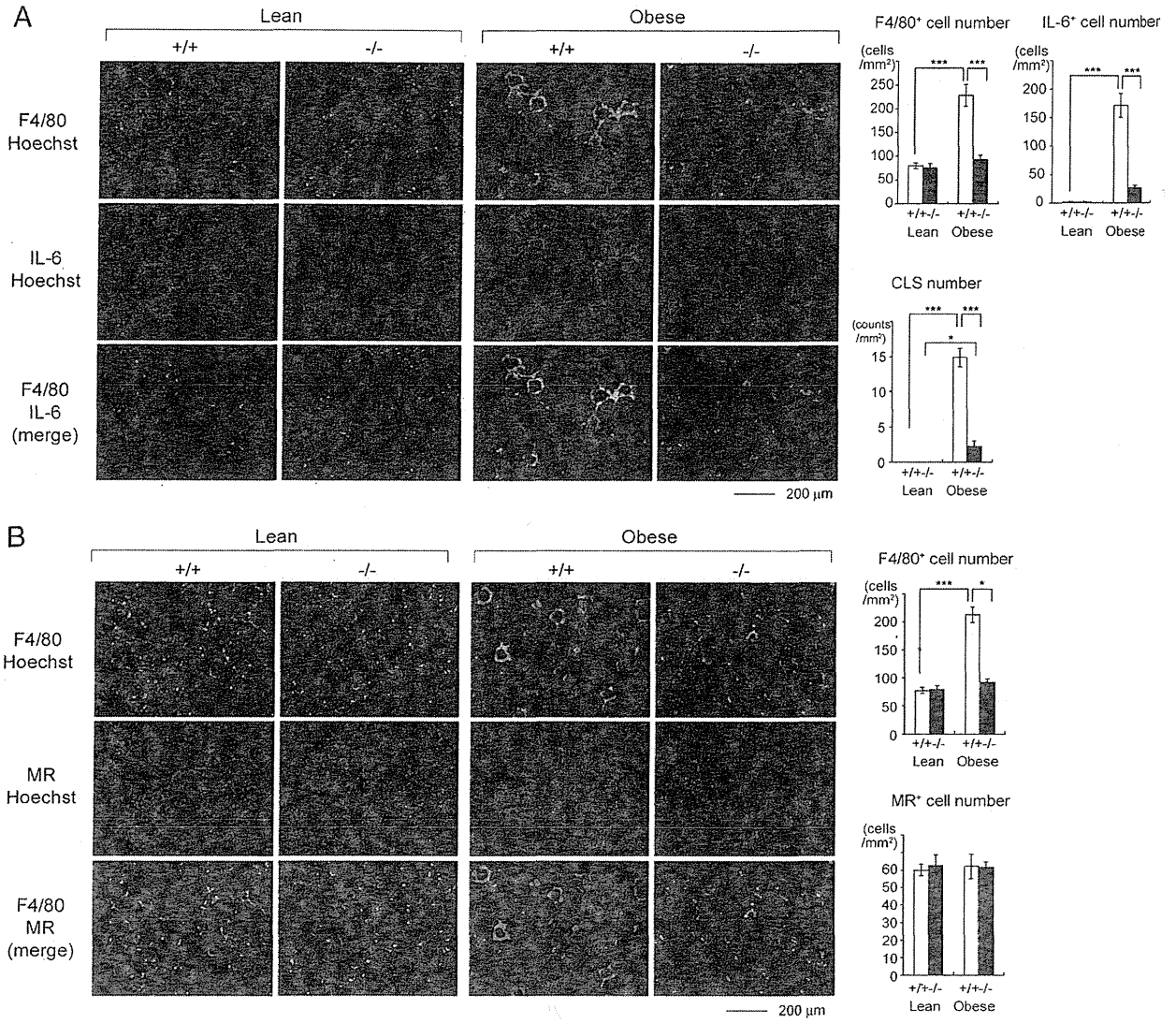

Fig. 1. Requirement of AIM for macrophage recruitment into obese adipose tissue. (*A* and *B*) Specimens of epididymal fat tissue from lean (0 wk) or obese (fed a HFD for 12 wk) $AIM^{+/+}$ and $AIM^{-/-}$ mice were costained for F4/80 (pan-macrophage marker; green), IL-6 (red), and Hoechst (blue) for *A*, and F4/80 (pan-macrophage marker; green), mannose receptor (MR) (red), and Hoechst (blue) for *B*. (Scale bar, 200 μm.) Quantification of F4/80⁺ cell number, IL-6⁺ macrophages, and the number of crown-like structures (CLS) are presented for *A*, or F4/80⁺ cell number and MR⁺ macrophages for *B* are presented. At least three different areas in three different sections per mouse were analyzed in six to eight mice of each genotype. Results are presented as averages ± SEM.

assessed to determine the number of both types of macrophage by flow cytometry after staining for F4/80 and CD11b (macrophage), CD11c (M1 marker), and MR. Consistent with the histological data, the increase in M1 macrophage number was apparent in obese $AIM^{+/+}$ but not in obese $AIM^{-/-}$ mice (Fig. S1*A*). The M1/M2 ratio of macrophage number was significantly increased in obese $AIM^{+/+}$ than in lean $AIM^{+/+}$ mice, indicating M1 polarization of adipose tissue macrophage (9), whereas this was comparable in lean and obese $AIM^{-/-}$ mice (Fig. S1*B*). Similarly, quantitative RT-PCR (QPCR) analysis with RNA isolated from epididymal fat showed a remarkable increase in mRNA levels for M1 macrophage marker genes, such as *CD11c* and *iNOS*, after a 12-wk HFD in $AIM^{+/+}$ mice, whereas this was not apparent in $AIM^{-/-}$ mice (Fig. S1*C*). In addition, expression levels of antiinflammatory (M2) macrophage marker genes, such as *CD163*, *MR*, and *arginase*, were decreased in epididymal fat of $AIM^{+/+}$ mice fed a HFD, whereas this was not observed in $AIM^{-/-}$ mice (Fig. S1*C*). The reduction in mRNA levels of M2 markers in obese $AIM^{+/+}$ mice is consistent with the increase in the M1/M2 ratio of macrophage number in obese $AIM^{+/+}$ mice (Fig. 1*D*). The difference in macrophage accumulation in fat in the presence or absence of AIM was not predominantly brought about by the antiapoptotic effect of AIM (13, 20) because the apoptotic state of macrophages (and also of adipocytes) was comparable between obese $AIM^{+/+}$ and $AIM^{-/-}$ epididymal adipose tissues, as assessed by TUNEL staining (Fig. S2). These results implicate an indispensable role of AIM in the obesity-associated recruitment of adipose tissue macrophages.

AIM-Dependent Lipolysis Induces Macrophage Migration. We then tested whether AIM itself attracts macrophages. However, AIM showed no chemoattractive activity in a macrophage migration assay using RAW264.1 mouse macrophage cells (Fig. 2*A*, *Left*). In contrast, conditioned medium from 3T3-L1 adipocytes that had been challenged with rAIM for 72 h (AIM CM) efficiently attracted macrophage cells (Fig. 2*A*, *Left*). A comparable effect was observed with conditioned medium from cells treated with C75, a specific FAS inhibitor that also induces lipolysis (14). AIM CM also attracted

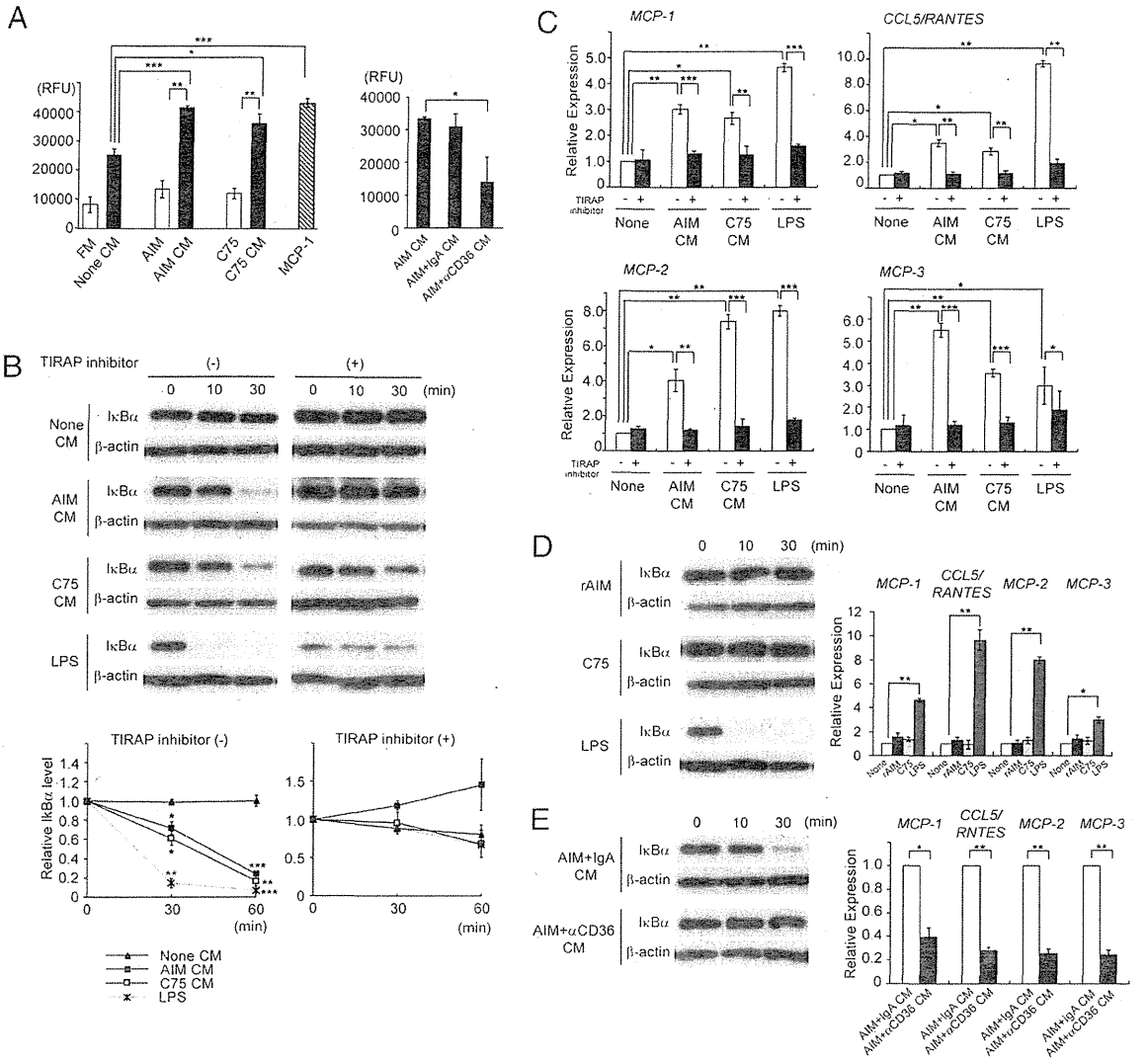

Fig. 2. AIM-dependent lipolysis induces chemokine production in adipocytes via TLR4 stimulation. (*A*) Chemotaxis of RAW 264.1 cells in response to specified stimulant. Attractants: rAIM (25 μg/mL), C75 (25 μM), AIM CM/C75 CM: conditioned medium from 3T3-L1 adipocytes treated for 3 d with rAIM (25 μg/mL) or C75 (25 μM), respectively; AIM+αCD36 CM/AIM+IgA CM: conditioned medium from 3T3-L1 adipocytes treated for 3 d with rAIM (25 μg/mL) in the presence of anti-CD36 Ab or mouse IgA (10 μg/mL each), respectively; none CM, control CM: treated without rAIM or C75; and FM: fresh DMEM culture medium containing 10% FBS. Averages from $n = 3 \pm$ SEM. MCP-1 (100 ng/mL) was used as a positive control. (*B*) Degradation of IkBα in 3T3-L1 adipoctytes in response to specified stimulant in the absence (–) or presence (+) of a TIRAP inhibitor (100 μM). LPS (100 ng/mL) was used as a positive control. Representative immunoblotting results are presented. The density of the signal was quantified using National Institutes of Health Image J image analysis software and presented as values relative to those of prestimulation (*Lower* two panels). $n = 3$. Error bar: SEM. *, versus the value at prestimulation (0 min). (*C*) QPCR analysis of mRNA levels for *MCP-1, CCL5/RANTES, MCP-2,* and *MCP-3* using RNA isolated from 3T3-L1 adipocytes treated with specified stimulant for 24 h in the absence (white bars) or presence (black bars) of a TIRAP inhibitor. Values were presented as relative expression to those without stimulation (none). $n = 3$ for each. Error bar: SEM. (*D* and *E*) No degradation of IkBα or expression induction of mRNA for chemokine genes in 3T3-L1 adipoctytes in response to rAIM alone (25 μg/mL) (*D*) or AIM+αCD36 CM (*E*).

J774.1 mouse monocyte cells (Fig. S3*A*). Furthermore, 3T3-L1 adipocytes were treated with rAIM in the presence of a CD36-neutralizing antibody (mouse IgA), which inhibits AIM-dependent lipolysis by disturbing the endocytosis of AIM into adipocytes (14), and the conditioned medium (AIM+αCD36 CM) was assessed in the macrophage migration assay. The AIM+αCD36 CM did not efficiently attract macrophages (Fig. 2*A*, *Right*), suggesting that AIM-induced lipolysis in adipocytes appears to be responsible for macrophage recruitment. The CD36-neutralizing antibody itself had no direct effect on the macrophage migration (Fig. S3*B*).

Fatty Acids Effluxed from Adipocytes in Response to AIM-Dependent Lipolysis Stimulated TLR Signaling Pathway and Induced Chemokine Production in Adipocytes. Accumulating evidence has demonstrated that saturated fatty acids activate TLR signaling cascade and that this response is tightly associated with obesity-induced inflammation (21–25). Thus, it is plausible that an increase in blood AIM may induce vigorous lipolysis in obese adipose tissues, and saturated fatty acids effluxed from adipocytes as a result of lipolysis might activate chemokine production in adipocytes via the stimulation of TLR(s) in a paracrine/autocrine fashion (26–28). Indeed, palmitic and stearic acids, the major fatty acids comprising triglyceride droplets (29) and well known as stimulators of TLR4 and TLR2 (21, 25, 30, 31), were identified as the components released by adipocytes in response to lipolysis induced by AIM or C75 when the profile of fatty acids in AIM CM and C75 CM was evaluated by gas-chromatography mass-spectrometry analysis.

Consistent with this result, both AIM CM and C75 CM efficiently stimulated the TLR signaling cascade and chemokine production in 3T3-L1 adipocytes, as assessed by degradation of IkBα (Fig. 2*B*) and mRNA expression of chemokines such as *MCP-1*, *CCL5/RANTES*, *MCP-2*, and *MCP-3*, which affects macrophages (Fig. 2*C*). AIM CM induced substantial levels of protein of these chemokines as assessed by ELISA (Fig. S4*A*). These responses diminished when adipocytes were treated with AIM CM or C75 CM in the presence of a toll–interleukin-1 receptor domain containing adapter protein (TIRAP) inhibitor, which specifically interferes with the interaction of TLR4 (as well as TLR2) and the adapter protein TIRAP/Mal, resulting in attenuation of TLR signaling (Fig. 2 *B* and *C*) (32). Furthermore, we confirmed that similar effects of TLR activation and chemokine production were observed when 3T3-L1 adipocytes were treated with palmitic acid (PA) or stearic acid (SA) and that the responses induced by each fatty acid were reduced when subjected to the TIRAP inhibitor (Fig. S5). Consistent with the results from macrophage migration assay presented in Fig. 2*A*, neither rAIM alone (Fig. 2*D* and Fig. S4*B*) nor AIM+αCD36 CM (Fig. 2*E* and Fig. S4*C*) stimulated IkBα degradation or chemokine mRNA and protein expression in adipocytes. These findings clearly indicate the necessity of the lipolytic process in the overall activation of TLR signaling cascade by AIM.

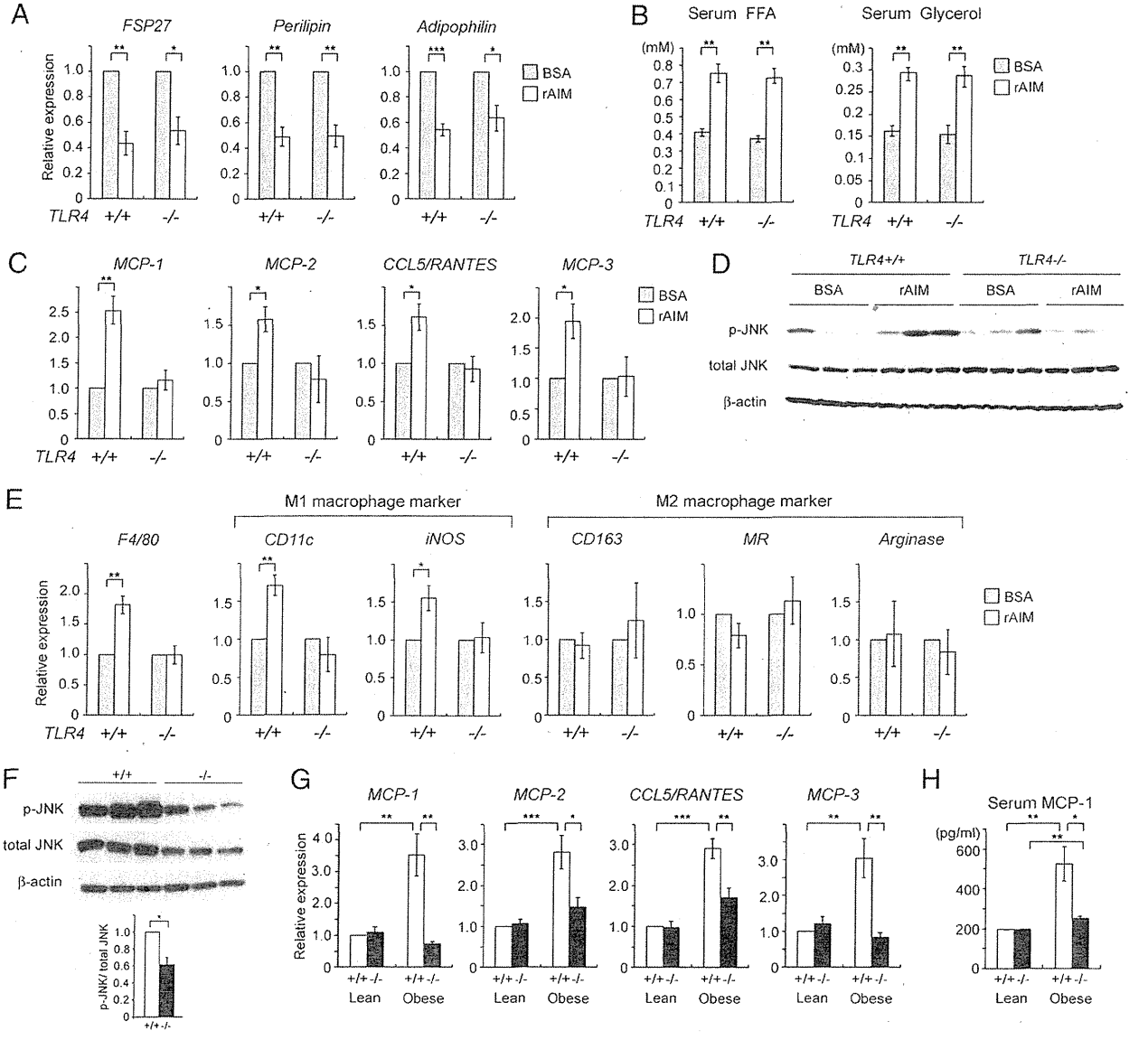

Fig. 3. Involvement of TLR4 in adipose tissue macrophage recruitment by AIM in vivo. (*A–E*) *TLR4*$^{-/-}$ and wild-type littermate mice (B6 background) were i.v. injected with rAIM or BSA three times every other day (400 μg in 200 μL PBS per injection). The day after the third injection (day 8 from the first injection), mice were killed, and lipolysis, chemokine expression, and adipose tissue macrophage accumulation were analyzed. $n = 5$ for each. (*A*) mRNA levels for *FSP27*, *Perilipin*, and *Adipophilin* were assessed by QPCR using RNA isolated from epididymal fat. Values were presented as relative expression to those of fat tissue injected with BSA. Error bar: SEM. (*B*) Serum levels for FFA and glycerol. (*C*) mRNA levels for chemokines. (*D*) Immunoblotting for total and phosphorylated JNK in epididymal fat. Immunoblot for β-actin is also presented. Results from three mice for each group are presented. Note that comparable results were obtained in five independent mice in each group. (*E*) mRNA levels for F4/80 pan-macrophage marker, M1 and M2 macrophage markers to assess macrophage recruitment. (*F*) Immunoblotting for total and phosphorylated JNK using lysates obtained from epididymal fats of *AIM*$^{+/+}$ and *AIM*$^{-/-}$ mice fed a HFD for 12 wk ($n = 4–6$). Relative values of phosphorylated JNK signals to total JNK are also presented (*Lower* graph). (*G*) QPCR analysis of mRNA levels for chemokine genes in epididymal fat tissue and (*H*) serum MCP-1 concentration in *AIM*$^{+/+}$ and *AIM*$^{-/-}$ mice fed a HFD for 0 (lean) or 12 wk (obese); $n = 6–8$.

Involvement of TLR4. As TIRAP is downstream of not only TLR4 but also other TLRs, including TLR2 (32), the precise involvement of TLR4 in macrophage recruitment was further verified. We first suppressed *TLR4* expression by siRNA in 3T3-L1 adipocytes and assessed the induction of MCP-1 by AIM CM. As shown in Fig. S6 *A–C*, induction of both mRNA and protein of MCP-1 by AIM CM was significantly reduced in cells transfected with siRNA for *TLR4*. In addition, we injected rAIM i.v. into wild-type and $TLR4^{-/-}$ mice and thereafter assessed the state of lipolysis and chemokine production in epididymal adipose tissue. In both types of mice, the mRNA levels of *FSP27* (also called *Cidec*), *Perilipin*, and *Adipophilin*, coating elements for lipid droplets, were decreased after challenging with rAIM (Fig. 3*A*), a finding consistent with the progression of lipolysis reported previously (17, 33, 34). Similarly, the increase in blood FFA and glycerol levels was equivalent in $TLR4^{-/-}$ and wild-type mice (Fig. 3*B*). In contrast, induction of mRNA for chemokines by rAIM injection was significantly less efficient in $TLR4^{-/-}$ than in wild-type mice (Fig. 3*C*). In line with this, phosphorylation levels of c-Jun N-terminal kinases (JNKs) in epididymal fat, which represent the state of TLR activation, were up-regulated in wild-type mice but not in $TLR4^{-/-}$ mice (Fig. 3*D*). Furthermore, the rAIM injection increased mRNA levels for M1 macrophage markers in epididymal adipose tissue of wild-type but not $TLR4^{-/-}$ mice, demonstrating that AIM-induced lipolysis could not recruit inflammatory macrophages into adipose tissue in the absence of TLR4 (Fig. 3*E*). There was no significant change in mRNA levels for M2 macrophage markers in both $TLR4^{-/-}$ and wild-type mice (Fig. 3*E*). Histological analysis revealed the presence of IL-6 expressing M1 macrophages after the rAIM injection in epididymal adipose tissue of wild-type mice but not of $TLR4^{-/-}$ mice (Fig. S6*D*).

Consistent results were obtained in obese $AIM^{+/+}$ and $AIM^{-/-}$ mice after 12 wk on a HFD. In epididymal fat, phosphorylation levels of JNKs were decreased in $AIM^{-/-}$ mice compared with $AIM^{+/+}$ mice (Fig. 3*F*). In addition, chemokine mRNA levels were also lower in $AIM^{-/-}$ than in $AIM^{+/+}$ adipose tissue (Fig. 3*G*). Moreover, the serum level of MCP-1 was lower in $AIM^{-/-}$ than in $AIM^{+/+}$ mice (Fig. 3*H*).

It is possible that fatty acids effluxed from adipocytes may stimulate TLR4 expressed not only on adipocytes but also on resident M2 macrophages within adipose tissue in a paracrine fashion and may induce chemokine expression in macrophages. To assess this possibility, we stained epididymal fat from wild-type $AIM^{+/+}$ mice fed a HFD for 6 wk for MR, a M2 macrophage marker, and MCP-1. As shown in Fig. S7, both adipocytes and M2 macrophages stained positive for MCP-1. As expected, in $AIM^{-/-}$ mice, neither adipocytes nor resident macrophages showed obvious MCP-1 expression. Thus, in summary, AIM-induced lipolysis provoked the efflux of saturated fatty acids, including palmitic and stearic acids, from adipocytes, and these fatty acids stimulated chemokine production in both adipocytes and resident macrophages via TLR4 activation, resulting in M1 macrophage migration.

Prevention of Obesity-Associated Inflammation and Insulin Resistance in $AIM^{-/-}$ Mice. As a consequence of abolished infiltration of inflammatory macrophages, the progression of obesity-associated inflammation was prevented both locally and systemically in obese $AIM^{-/-}$ mice. In adipose tissue (Fig. 4*A*) and the liver (Fig. S8), mRNA levels for proinflammatory cytokines, such as *TNFα*, *IL-6*, and *IL-1β*, were significantly lower in $AIM^{-/-}$ than in $AIM^{+/+}$ mice after a HFD for 12 wk. Consistent with this finding, serum levels of TNFα and IL-6 were lower in $AIM^{-/-}$ mice compared with $AIM^{+/+}$mice (Fig. 4*B*).

Having observed decreased inflammation in $AIM^{-/-}$ mice, we next assessed insulin sensitivity in $AIM^{-/-}$ and $AIM^{+/+}$ mice fed a HFD for 12 wk. Activation of the insulin signaling pathway after i.v. injection of insulin was studied in adipose tissue, skeletal muscle (gastrocnemius), and liver. As shown in Fig. 4*C*, substantial insulin-stimulated phosphorylation of AKT and GSK3β protein kinases

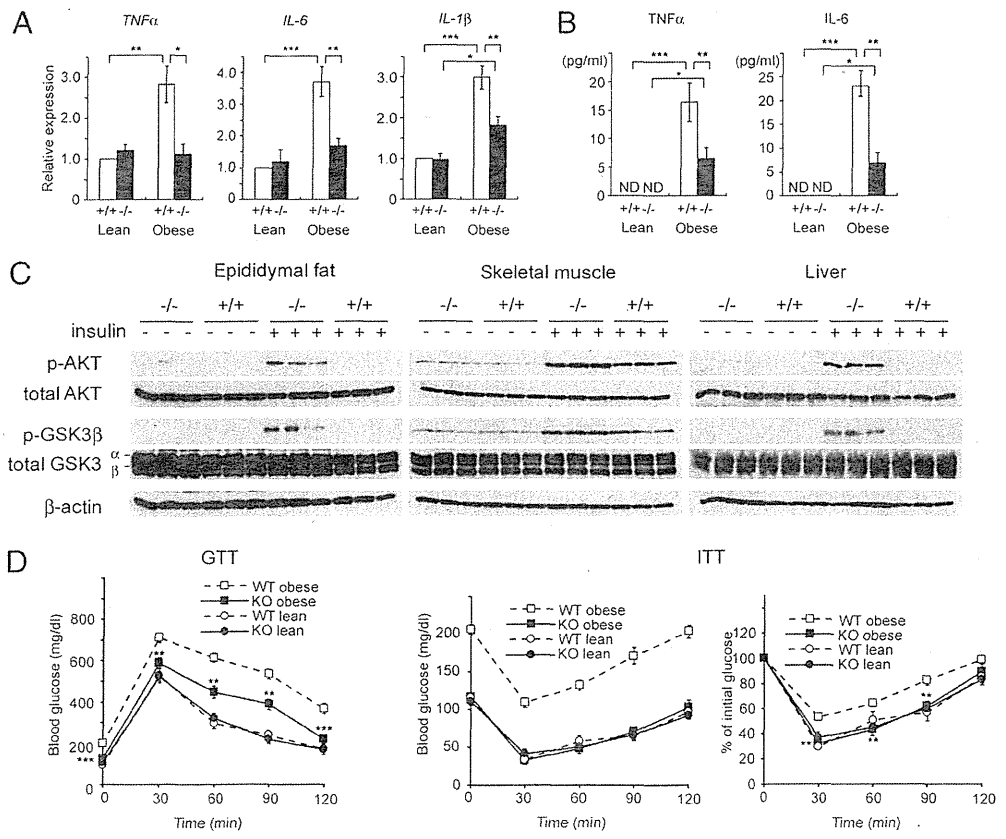

Fig. 4. Prevented inflammation and normal insulin sensitivity in obese $AIM^{-/-}$ mice. (*A*) Local inflammation. QPCR analysis of mRNA levels for inflammatory cytokine genes in epididymal fat tissue from $AIM^{+/+}$ or $AIM^{-/-}$ mice fed a HFD for 0 (lean) or 12 wk (obese). n = 6–8 for each group. Values were presented as relative expression to that in lean $AIM^{+/+}$ mice. Error bar: SEM. (*B*) Systemic inflammation. Serum TNFα and IL-6 levels are the same as in *A*. (*C*) $AIM^{-/-}$ and $AIM^{+/+}$ mice fed a HFD for 12 wk (three mice for each) were fasted for 5 h and treated with insulin (10 U/kg body weight) via i.p. injection. Within 15 min, epididymal fat, skeletal muscle (gastrocnemius), and liver were isolated and examined by immunoblotting for phosphorylated AKT (p-AKT), total AKT, phosphorylated GSK3β (p-GSK3β), total GSK3 (α and β), and β-actin. (*D*) Glucose tolerance test (GTT) and insulin tolerance test (ITT) performed on $AIM^{+/+}$ and $AIM^{-/-}$ mice fed a HFD for 0 (lean) or 12 wk (obese); n = 6–8 for each group. For ITT, two panels including absolute blood glucose levels (*Left*) and % of the initial (time 0) glucose level (*Right*) are presented.

was observed in all three tissues in $AIM^{-/-}$ mice in contrast to the markedly diminished phosphorylation levels in $AIM^{+/+}$ mice. Thus, insulin sensitivity was preserved in obese $AIM^{-/-}$ mice. Consistent with these results, whole-body glucose intolerance and insulin resistance observed in $AIM^{+/+}$ mice were found to be ameliorated in $AIM^{-/-}$ mice by i.p. glucose and insulin tolerance tests (GTT and ITT, respectively; Fig. 4*D*). Insulin production in pancreatic β cells in response to glucose was comparable in $AIM^{-/-}$ and $AIM^{+/+}$ mice, as assessed in vivo (Fig. S8*B*) and in vitro using isolated pancreatic Langerhans islets (Fig. S8*C*).

Conclusion

The present results provide unique and important evidence regarding the role of AIM in the initiation of chronic inflammation that connects obesity and insulin resistance. Firstly, macrophage recruitment into obese adipose tissues requires AIM-induced lipolysis. Augmentation of blood AIM levels may induce vigorous lipolysis in obese adipose tissues, increasing local extracellular fatty acid concentration to a level sufficient for the stimulation of TLR4, which triggers chemokine production by adipocytes and macrophage recruitment (summarized in Fig. S9). Although we and others previously reported some related facts underlying this conclusion, which were observed in a number of different physiological and experimental conditions (12, 14, 21–33), we would like to emphasize that this study, which focused on AIM, has uniquely linked apparently independent elements to a process that occurs during the progression to obesity.

Secondly, adipocyte hypertrophy is not solely sufficient for the initiation of macrophage infiltration; an increase in blood AIM needs to be accompanied. In $AIM^{-/-}$ mice, although the level of AIM-independent lipolysis increases in line with adipocyte hypertrophy (14), it may not reach a level sufficient for macrophage recruitment (Fig. S9). Thirdly, within adipose tissue, crosstalk between macrophages and adipocytes establishes a vicious cycle that accelerates inflammation; saturated fatty acids brought about by lipolysis activate TLR4 to induce TNFα, which in turn activates the TNFα receptor to produce inflammatory cytokines/adipokines and chemokines (35). The end point of this response is further progression of inflammation, lipolysis, and macrophage recruitment. It is likely that via an increase in lipolysis, AIM may strengthen this crosstalk, further contributing to the progression of inflammation (Fig. S9).

Thus, this study might not only advance our knowledge about the events triggering obesity-associated inflammation, but also open a door to the development of next-generation antimetabolic therapies via suppression of AIM.

Materials and Methods

Mice. $AIM^{-/-}$ mice (13) had been backcrossed to C57BL/6 (B6) for 13 generations before used for experiments. HFD (HFD32, fat kcal: 60%) was purchased from CREA. $TLR4^{-/-}$ mice (36) were kindly provided from Drs. S. Akira (Osaka University, Osaka, Japan) and K. Miyake (The Institute of Medical Science, University of Tokyo, Tokyo, Japan). All mice were maintained under a specific pathogen free condition.

Statistical Analysis. A two-tailed Mann-Whitney test was used to calculate *P* values. $***P < 0.001$, $**P < 0.01$, $*P < 0.05$. Error bars: SEM.

Please see *SI Materials and Methods* for further details.

ACKNOWLEDGMENTS. We thank Genostaff Inc. for technical assistance in histology. This work was supported by Grants-in-Aid for Scientific Research (B) (Japan Society for the Promotion of Science), the Global Centers of Excellence (COE) Program (T.M.), Kanae Foundation for the Promotion of Medical Science, the Astellas Foundation for Research on Metabolic Disorders, and the Ono Medical Research Foundation (S.A.).

1. Hotamisligil GS, Shargill N-S, Spiegelman B-M (1993) Adipose expression of tumor necrosis factor-alpha: Direct role in obesity-linked insulin resistance. *Science* 259: 87–91.
2. Wellen KE, Hotamisligil GS (2003) Obesity-induced inflammatory changes in adipose tissue. *J Clin Invest* 112:1785–1788.
3. Arkan MC, et al. (2005) IKK-beta links inflammation to obesity-induced insulin resistance. *Nat Med* 11:191–198.
4. Shoelson SE, Lee J, Goldfine AB (2006) Inflammation and insulin resistance. *J Clin Invest* 116:1793–1801.
5. Weisberg SP, et al. (2003) Obesity is associated with macrophage accumulation in adipose tissue. *J Clin Invest* 112:1796–1808.
6. Xu H, et al. (2003) Chronic inflammation in fat plays a crucial role in the development of obesity-related insulin resistance. *J Clin Invest* 112:1821–1830.
7. Solinas G, et al. (2007) JNK1 in hematopoietically derived cells contributes to diet-induced inflammation and insulin resistance without affecting obesity. *Cell Metab* 6: 386–397.
8. Gordon S, Taylor PR (2005) Monocyte and macrophage heterogeneity. *Nat Rev Immunol* 5:953–964.
9. Lumeng CN, Bodzin JL, Saltiel AR (2007) Obesity induces a phenotypic switch in adipose tissue macrophage polarization. *J Clin Invest* 117:175–184.
10. Ozcan U, et al. (2004) Endoplasmic reticulum stress links obesity, insulin action, and type 2 diabetes. *Science* 306:457–461.
11. Kahn SE, Hull RL, Utzschneider KM (2006) Mechanisms linking obesity to insulin resistance and type 2 diabetes. *Nature* 444:840–846.
12. Kosteli A, et al. (2010) Weight loss and lipolysis promote a dynamic immune response in murine adipose tissue. *J Clin Invest* 120:3466–3479.
13. Miyazaki T, Hirokami Y, Matsuhashi N, Takatsuka H, Naito M (1999) Increased susceptibility of thymocytes to apoptosis in mice lacking AIM, a novel murine macrophage-derived soluble factor belonging to the scavenger receptor cysteine-rich domain superfamily. *J Exp Med* 189:413–422.
14. Kurokawa J, et al. (2010) Macrophage-derived AIM is endocytosed into adipocytes and decreases lipid droplets via inhibition of fatty acid synthase activity. *Cell Metab* 11:479–492.
15. Joseph SB, et al. (2004) LXR-dependent gene expression is important for macrophage survival and the innate immune response. *Cell* 119:299–309.
16. Valledor AF, et al. (2004) Activation of liver X receptors and retinoid X receptors prevents bacterial-induced macrophage apoptosis. *Proc Natl Acad Sci USA* 101: 17813–17818.
17. Gebe JA, et al. (1997) Molecular cloning, mapping to human chromosome 1 q21-q23, and cell binding characteristics of Spalpha, a new member of the scavenger receptor cysteine-rich (SRCR) family of proteins. *J Biol Chem* 272:6151–6158.
18. Kim WK, et al. (2008) Glycoproteomic analysis of plasma from patients with atopic dermatitis: CD5L and ApoE as potential biomarkers. *Exp Mol Med* 40:677–685.
19. Gray J, et al. (2009) A proteomic strategy to identify novel serum biomarkers for liver cirrhosis and hepatocellular cancer in individuals with fatty liver disease. *BMC Cancer* 9:271.
20. Arai S, et al. (2005) A role for the apoptosis inhibitory factor AIM/Spalpha/Api6 in atherosclerosis development. *Cell Metab* 1:201–213.
21. Shi H, et al. (2006) TLR4 links innate immunity and fatty acid-induced insulin resistance. *J Clin Invest* 116:3015–3025.
22. Suganami T, et al. (2007) Role of the Toll-like receptor 4/NF-kappaB pathway in saturated fatty acid-induced inflammatory changes in the interaction between adipocytes and macrophages. *Arterioscler Thromb Vasc Biol* 27:84–91.
23. Poggi M, et al. (2007) C3H/HeJ mice carrying a toll-like receptor 4 mutation are protected against the development of insulin resistance in white adipose tissue in response to a high-fat diet. *Diabetologia* 50:1267–1276.
24. Tsukumo DM, et al. (2007) Loss-of-function mutation in Toll-like receptor 4 prevents diet-induced obesity and insulin resistance. *Diabetes* 56:1986–1998.
25. Davis JE, Gabler NK, Walker-Daniels J, Spurlock ME (2008) Tlr-4 deficiency selectively protects against obesity induced by diets high in saturated fat. *Obesity (Silver Spring)* 16:1248–1255.
26. Kamei N, et al. (2006) Overexpression of monocyte chemoattractant protein-1 in adipose tissues causes macrophage recruitment and insulin resistance. *J Biol Chem* 281:26602–26614.
27. Kanda H, et al. (2006) MCP-1 contributes to macrophage infiltration into adipose tissue, insulin resistance, and hepatic steatosis in obesity. *J Clin Invest* 116:1494–1505.
28. Keophiphath M, Rouault C, Divoux A, Clément K, Lacasa D (2010) CCL5 promotes macrophage recruitment and survival in human adipose tissue. *Arterioscler Thromb Vasc Biol* 30:39–45.
29. Soma MR, Mims MP, Chari MV, Rees D, Morrisett JD (1992) Triglyceride metabolism in 3T3-L1 cells. An in vivo 13C NMR study. *J Biol Chem* 267:11168–11175.
30. Kopp A, et al. (2009) Fatty acids as metabolic mediators in innate immunity. *Eur J Clin Invest* 39:924–933.
31. Schaeffler A, et al. (2009) Fatty acid-induced induction of Toll-like receptor-4/nuclear factor-kappaB pathway in adipocytes links nutritional signalling with innate immunity. *Immunology* 126:233–245.
32. Jenkins KA, Mansell A (2010) TIR-containing adaptors in Toll-like receptor signalling. *Cytokine* 49:237–244.
33. Zechner R, Strauss JG, Haemmerle G, Lass A, Zimmermann R (2005) Lipolysis: Pathway under construction. *Curr Opin Lipidol* 16:333–340.
34. Nishino N, et al. (2008) FSP27 contributes to efficient energy storage in murine white adipocytes by promoting the formation of unilocular lipid droplets. *J Clin Invest* 118: 2693–2696.
35. Schäffler A, Schölmerich J, Salzberger B (2007) Adipose tissue as an immunological organ: Toll-like receptors, C1q/TNFs and CTRPs. *Trends Immunol* 28:393–399.
36. Hoshino K, et al. (1999) Cutting edge: Toll-like receptor 4 (TLR4)-deficient mice are hyporesponsive to lipopolysaccharide: Evidence for TLR4 as the Lps gene product. *J Immunol* 162:3749–3752.

Biochemical and Biophysical Research Communications 415 (2011) 545–550

Contents lists available at SciVerse ScienceDirect

Biochemical and Biophysical Research Communications

journal homepage: www.elsevier.com/locate/ybbrc

IRS-2 deficiency in macrophages promotes their accumulation in the vascular wall

Tomoya Mita [a], Kosuke Azuma [a], Hiromasa Goto [a], Wen long Jin [a], Masayuki Arakawa [a], Takashi Nomiyama [a], Ryo Suzuki [e], Naoto Kubota [e], Kazuyuki Tobe [f], Takashi Kadowaki [e], Yoshio Fujitani [a,c], Takahisa Hirose [a,c], Ryuzo Kawamori [a,b,c,d], Hirotaka Watada [a,b,c,d,*]

[a] Department of Medicine, Metabolism and Endocrinology, Juntendo University Graduate School of Medicine, Tokyo 113-8421, Japan
[b] Sportology Center, Juntendo University Graduate School of Medicine, Tokyo 113-8421, Japan
[c] Center for Therapeutic Innovations in Diabetes, Juntendo University Graduate School of Medicine, Tokyo 113-8421, Japan
[d] Center for Beta Cell Biology and Regeneration, Juntendo University Graduate School of Medicine, Tokyo 113-8421, Japan
[e] Department of Metabolic Diseases, Graduate School of Medicine, University of Tokyo, Tokyo 113-8655, Japan
[f] First Department of Internal Medicine, University of Toyama, Toyama 930-0194, Japan

ARTICLE INFO

Article history:
Received 4 October 2011
Available online 2 November 2011

Keywords:
Atherosclerosis
Diabetes mellitus
Insulin
Inflammation
Macrophage

ABSTRACT

The aim of this study was to investigate the role of insulin receptor substrate-2 (IRS-2) mediated signal in macrophages on the accumulation of macrophages in the vascular wall. Mice transplanted with IRS-2$^{-/-}$ bone marrow, a model of myeloid cell restricted defect of IRS-2, showed accumulation of monocyte chemoattractant protein-1-expressing macrophages in the vascular wall. Experiments using cultured peritoneal macrophages showed that IRS-2-mediated signal pathway stimulated by physiological concentrations of insulin, not by IL-4, contributed to the suppression of monocyte chemoattractant protein-1 expression induced by lipopolysaccharide. Our data indicated that IRS-2 deficiency in macrophages enhanced their accumulation in the vascular wall accompanied by increased expression of proinflammatory mediators in macrophages. These results suggest a role for insulin resistance in macrophages in early atherosclerogenesis.

1. Introduction

Diabetes is a major risk factor for cardiovascular disease, but the underlying mechanism remains poorly understood. Epidemiological studies identified insulin resistance or hyperinsulinemia as an independent risk factor for cardiovascular disease [1,2].

In addition to serum risk factors induced by systemic insulin resistance, recent studies demonstrated that insulin resistance at cellular level, including endothelial cells [3,4], and vascular smooth muscle cells [5], may accelerate atherosclerosis. Monocytes/macrophages also express the majority of insulin signal molecules [6], thus, they are regarded as a target in which insulin resistance may be associated with the progression of atherosclerosis. We reported recently that monocytes/macrophages with reduced insulin signaling exhibit enhanced adherence to the endothelium of inflamed vascular wall, in the presence of systemic insulin resistance [7]. However, the direct role of insulin signaling in monocytes/macrophages on the progression of atherosclerosis in the absence of systemic insulin resistance remains controversial [8–10].

In addition to the liver, muscle, fat, pancreatic beta cells, and lymphocytes, insulin receptor substrate-2 (IRS-2) is also expressed in macrophages [11]. It mediates intracellular signal pathways initiated by insulin, insulin growth factor-1 (IGF-1), and anti-inflammatory cytokines [11]. Recent studies reported that insulin can inhibit the production of proinflammatory cytokines in human aortic endothelial cells [12], mononuclear cells [13] and alveolar macrophages [14]. In contrast, reduced insulin signal in macrophages enhances the production of inflammatory cytokines [15,16]. Furthermore, interleukin-4 (IL-4), an important anti-inflammatory cytokine, is also known to inhibit the secretion of proinflammatory cytokines by macrophages and stimulate the production of anti-inflammatory molecules, such as IL-1 receptor antagonist (IL-1RA) and IL-1 receptor2 (IL-1R2) [11]. This intracellular signal is also mediated at least in part through the IRS-2/phosphatidylinositol 3-kinase pathway [11]. Thus, IRS-2 is a potentially important substrate that can drive macrophages towards an anti-inflammatory phenotype by insulin and IL-4 signaling. Intriguingly, low expression of IRS-2 was observed in macrophages of obese diabetic mice [8], however, its impact on early atherosclerotic changes has not been elucidated.

Abbreviations: LPS, lipopolysaccharide; MCP-1, monocyte chemoattractant protein-1.

* Corresponding author. Address: Department of Metabolism and Endocrinology, Juntendo University Graduate School of Medicine, 2-1-1 Hongo, Bunkyo-ku, Tokyo 113-8421, Japan. Fax: +81 3 3813 5996.
E-mail address: hwatada@juntendo.ac.jp (H. Watada).

0006-291X/$ - see front matter © 2011 Elsevier Inc. All rights reserved.
doi:10.1016/j.bbrc.2011.10.086

The present study was designed to determine the role of macrophage IRS-2 on the production of pro-inflammatory mediators and accumulation of macrophages in the vascular wall. For this purpose, we generated myeloid lineage cell-restricted IRS-2 deficient model using bone marrow transplantation. Unlike previous studies [10,17], this is the first study that investigated the impact of IRS-2 deficiency in macrophages not using mice with high LDL cholesterol levels.

2. Materials and methods

2.1. Animal experiments

The study protocol conformed the Guide for the Care and Use of Laboratory Animals published by the US National Institutes of Health. It was reviewed and approved by the Animal Care and Use Committee of Juntendo University. Male C57BL/6 mice were obtained from Jackson Laboratory at the age of 7 weeks. IRS-2 deficient (IRS-$2^{-/-}$) mice [18] on a mixed C57BL6 J/129sv background were backcrossed on C57BL/6 J background for generations. All mice were housed in a polycarbonate cage with a wooden chip mat on the floor. Water was available *ad libitum* for all mice. Normal chow was used in this study. The animal room was kept on a 12-h light/dark cycle (7:00 AM to 7:00 PM/light, 7:00 PM to 7:00 AM/dark), at constant temperature (22 ± 1 °C) and relative humidity of 55 ± 5% throughout the experiment. In some experiments, mice were injected intraperitoneally with 1 mg/kg lipopolysaccharide (LPS) as reported previously [19]. Mice were sacrificed by intraperitoneal injection of 1 mg/kg sodium pentobarbital.

2.2. Bone marrow transplantation

Bone marrow transplantation was performed as described previously [20,21]. Eight to nine-week-old male C57BL/6 mice were irradiated with a lethal dose of 1000 rads (10 Gy: 5 × 2). Recipient mice were treated with antibiotics (neomycin sulfate) added to the drinking water after irradiation for two weeks. The bone marrow was collected from the femurs and tibias of 8–9-week-old donor male C57BL/6 (IRS-$2^{+/+}$) or IRS-$2^{-/-}$ mice by flushing with sterile Dulbecco's Modified Eagle's Medium. Each recipient mouse was injected with about 5–6 × 10^6 bone marrow cells through the tail vein.

2.3. Laboratory data

Plasma glucose level was measured by glucose oxidase method using a compact glucose analyzer (One Touch Ultra Glucose Meter, Life Scan, Tokyo, Japan). Total cholesterol, HDL, LDL, and triglycerides were measured by an autoanalyzer (Hitachi, Tokyo).

2.4. Intraperitoneal glucose tolerance test and insulin tolerance test

Intraperitoneal glucose tolerance test and insulin tolerance test were performed by intraperitoneal injection of glucose (1.0 g/kg body weight) and regular insulin (0.75 units/kg body weight) (Humulin; Eli Lilly, Indianapolis, IN), respectively.

2.5. En face immunohistochemistry of endothelial surface

Mice were sacrificed by intraperitoneal injection of sodium pentobarbital (1 mg/kg; Abbott Laboratories). Fixation and tissue preparation were performed by systemic perfusion through the left ventricle, with 20 ml of normal saline followed by 10 ml of 10% buffered formalin. After fixation, the aorta from the aortic arch to the lower thoracic region was harvested for immunostaining with anti-mouse Mac-2 monoclonal antibody (Cedarlane, Burlington, ONT, Canada) using the procedure described previously [7,19, 22,23]. The density of Mac-2-immunopositive cells in the thoracic aorta was calculated as described previously [7,19,22,23]. For fluorescent staining, the sections were immunostained with rabbit polyclonal anti-monocyte chemoattractant protein-1(MCP-1) antibody (1:100, LS-A1205; MBL International Corporation, Woburn, MA) and rabbit anti-Mac-2 monoclonal antibody (1:100; Cedarlane). Samples were viewed under a confocal laser scanning microscope (Fluoview FV1000; Olympus, Tokyo).

2.6. Quantification of atherosclerotic lesions in the aortic sinus

The heart and aorta were flushed with normal saline followed by 10% buffered formalin. For quantitative analysis of the arteriosclerotic lesions in the aortic sinus, the heart was cut in two halves and the top half was embedded in optimal cutting temperature compound, then cross-sectioned into 4 μm thickness at 50 μm interval with a cryostat. Eight consecutive sections were taken sequentially from just above the aortic valve throughout the aortic sinus and allowed to dry at room temperature for 30 min, as described previously [7]. Sections were stained with Mac-2 antibody. Then, images were captured with ImagePro Plus software. The mean lesion area of those 8 sections was calculated and expressed the mean number of invaded macrophages.

2.7. Ex vivo treatment of macrophages

Peritoneal macrophages from the mice used in this study were harvested with cold phosphate-buffered saline at 3 days after intraperitoneal injection of sodium periodate, as reported previously [7]. The pooled macrophages from each mouse were cultured in Roswell Park Memorial Institute 1640, supplemented with or without 0.2% fetal calf serum, 2 mmol/L L-glutamine, 100 U/mL penicillin, 100 μg/mL streptomycin and 50 μM 2-mercaptoethanol, to allow cell adhesion. The nonadherent cells were removed by washing with phosphate-buffered saline. For experiments, freshly isolated macrophages were used followed by serum starvation for 2 h or overnight serum-starved macrophages were used. Serum-starved macrophages were washed once and then incubated without or with 10 or 100 pM insulin for 6 h, followed without or with 1 μg/ml LPS for 1 h. To investigate the effect of IL-4, serum-starved macrophages were washed once and then incubated without or with IL-4 (10 ng/ml) and LPS (10 ng/ml) for 6 h. Control macrophages were incubated with the vehicle, dimethyl sulfoxide (DMSO)(<0.1%, final concentration). After treatment, total RNA or cell lysates were prepared for further analysis.

2.8. Isolation of tissue RNA and real-time quantitative RT-PCR

Total RNA was extracted from the aorta using Trizol reagent (Invitrogen, Carlsbad, CA) and from peritoneal macrophages using RNAeasymicro Kit. To detect mouse IRS-2 gene expression in blood cells, blood samples were collected and total RNA was extracted using RNAeasy Kit (Qiagen, Tokyo) as described by the manufacturer. First strand cDNA was synthesized using 1 μg of total RNA with oligo-dT primers and superscript reverse transcriptase (Invitrogen), as described previously [7]. Then, the resulting cDNAs were amplified using the SYBER Green PCR kit (Applied Biosystems, Foster City, CA). Quantitative PCR was performed with an ABI Prism 7700 sequence detection system (Perkin Elmer Life Sciences, Boston, MA). The relative abundance of mRNAs was calculated by the comparative cycle of threshold method using TATA Box-binding protein for mice as the invariant control. The primer sequences used in this study were described previously [7].

2.9. Data analysis

Results are presented as mean ± SEM. Differences between two groups were examined for statistical significance using the unpaired Student's *t*-test. Comparisons of more than three groups were tested for statistical significance by one-way ANOVA and Scheffé's test as the post hoc test. A p value < 0.05 was considered significant.

3. Results

3.1. Accumulation of IRS-2-deficient macrophages in the vascular wall

In order to evaluate the impact of IRS-2 deficiency in macrophages on macrophage accumulation in the vascular wall, we generated myeloid lineage cell-restricted IRS-2 deficient model. Briefly, after lethal irradiation of 8- to 9-week old mice, the bone marrow from 8- to 9-week old-donor IRS2$^{-/-}$ or wild type mice was injected in the recipient. We named the established mice, ϕIRS-2$^{-/-}$ and ϕIRS-2$^{+/+}$ mice, respectively. The ϕIRS-2$^{-/-}$ mice showed 80% decrease in IRS-2 expression in blood cells (Fig. 1A). At 12 weeks after transplantation, body weight, glucose tolerance, insulin resistance and lipid profiles were comparable between the ϕIRS-2$^{-/-}$ and ϕIRS-2$^{+/+}$ mice (Fig. 1B–D and data not shown). However, the number of macrophages adherent to the endothelium was significantly higher in ϕIRS-2$^{-/-}$ mice than in ϕIRS-2$^{+/+}$ mice (Fig. 2A). In addition, ϕIRS-2$^{-/-}$ mice showed significant accumulation of macrophages in longitudinal sections of the aortic arch (Fig. 2B). While no significant increases in the expression of tumor necrosis factor-α (TNF-α), intercellular adhesion molecule 1 (ICAM-1), and vascular cell adhesion molecule-1 (VCAM-1) were observed in the thoracic aorta of ϕIRS-2$^{-/-}$ mice, the expression of MCP-1 was significantly higher in ϕIRS-2$^{-/-}$ mice than ϕIRS-2$^{+/+}$ mice (Fig. 2C). Macrophages isolated from ϕIRS-2$^{-/-}$ mice also expressed significantly higher levels of MCP-1 compared with ϕIRS-2$^{+/+}$ mice (Fig. 2D). Furthermore, the number of MCP-1 positive macrophages attached to the endothelium was higher in ϕIRS-2$^{-/-}$ mice than ϕIRS-2$^{+/+}$ mice (Fig. 2E). Taken together, these findings indicate that IRS-2 deficiency in macrophages *per se* promotes the accumulation of macrophages in the arterial wall in parallel with increased expression of MCP-1.

3.2. Reduced insulin-mediated IRS-2 signal in macrophages augments TNF-α and MCP-1 expression

To investigate the causal relationship between IRS-2 deficiency in macrophages and the expression of MCP-1, we explored the effects of insulin on mRNA expression levels of MCP-1 in macrophages. After serum starvation, peritoneal macrophages were incubated with various physiological concentrations of insulin (10–100 pM) for 6 h. As shown in Fig. 3A, physiological concentrations of insulin significantly suppressed the mRNA expression levels of MCP-1. We further explored whether the physiological concentrations of insulin protected against LPS-induced expression of MCP-1. Peritoneal macrophages were incubated with insulin for 6 h followed by incubation with LPS (1 μg/ml) for 1 h. While LPS stimulation induced 1.5 folds increase in MCP-1 expression (data not shown), physiological concentrations of insulin significantly suppressed LPS-induced MCP-1 expression. (Fig. 3B). In addition, the inhibitory effects of insulin on the expression of MCP-1 were completely abolished in IRS-2$^{-/-}$ macrophages (Fig. 3B).

IRS-2 is also known to mediate, at least in part, the anti-inflammatory effect of IL-4 [11]. While IL-4 suppressed LPS-induced MCP-1 expression, its suppression of MCP-1 expression in IRS-2$^{-/-}$ macrophages was comparable to that of IRS-2$^{+/+}$ macrophages (Fig. 3C). Taken together, these results indicate that IRS-2 mediates insulin signal, rather than IL-4 signal, and reduces the expression of MCP-1 in macrophages.

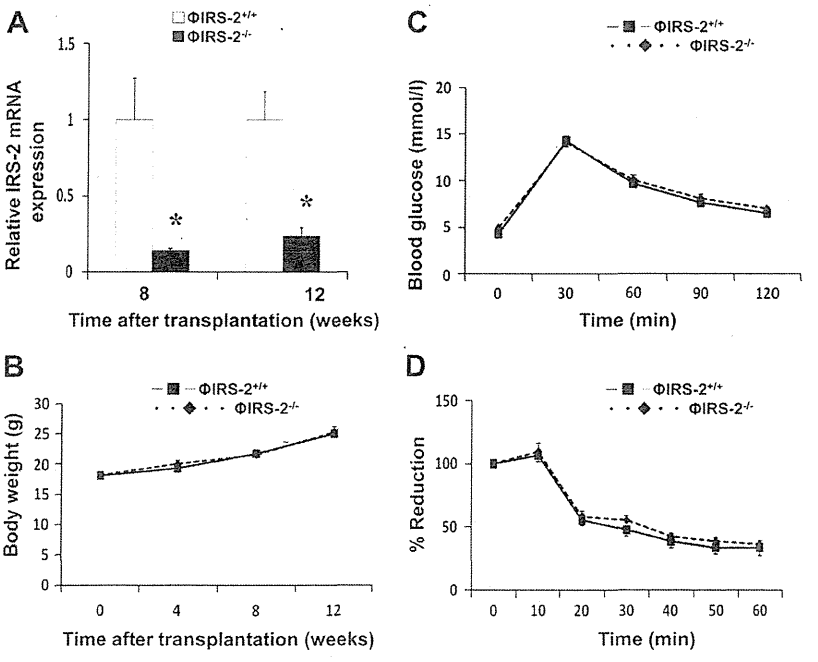

Fig. 1. Comparison of insulin sensitivity and glucose tolerance between ϕIRS-2$^{+/+}$ and ϕIRS-2$^{-/-}$ mice. (A) mRNA expression of IRS-2 in peripheral blood cells isolated from ϕIRS-2$^{+/+}$ and ϕIRS-2$^{-/-}$ mice at the indicated time after bone marrow transplantation. IRS-2 expression in blood cells from ϕIRS-2$^{+/+}$ mice at each age was set at 1.0. (B) Serial changes in body weight in the two groups of mice. (C) Results of intraperitoneal glucose tolerance tests conducted at 12 weeks after transplantation. (D) Insulin tolerance test conducted at 12 weeks after transplantation. Data are presented as% reduction in initial blood glucose level. All data are expressed as mean ± SEM (n = 7–8 mice). *P < 0.05 vs. ϕIRS-2$^{+/+}$ mice.

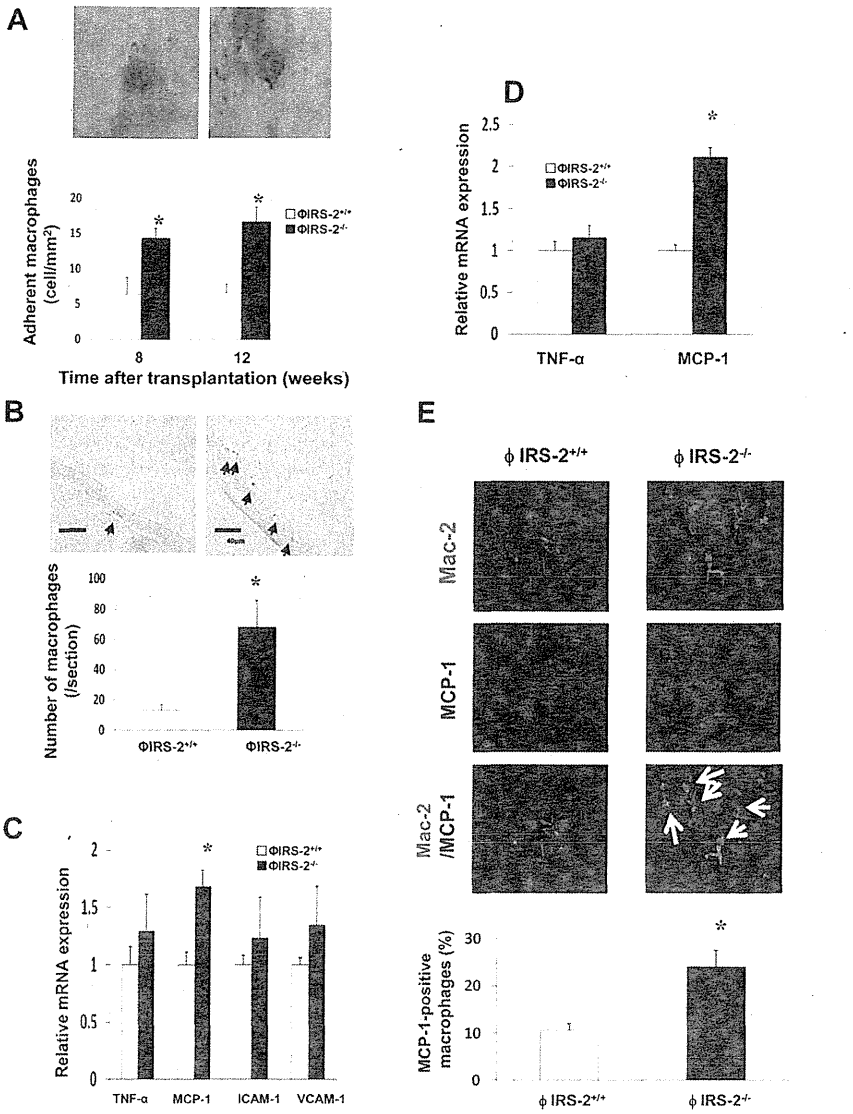

Fig. 2. Reduced IRS-2 signal in macrophages enhances the accumulation of monocytes/macrophages in the vascular wall. (A) Representative *en face* view of immunohistochemical staining with Mac2 antibody in the thoracic aortas of ϕIRS-$2^{+/+}$ and ϕIRS-$2^{-/-}$ mice at 8 weeks after the transplantation (upper panel). The density of adherent Mac2-positive cells on endothelial cells at branching areas was evaluated at 8 weeks ($n = 5$) and 12 weeks ($n = 9$) after transplantation (lower panel). (B) Representative micrographs of aortic cross-sections stained with Mac2 (upper panel). The number of macrophages per section was counted at 12 weeks after transplantation ($n = 7$) (lower panel). (C) Aortas were harvested from ϕIRS-$2^{+/+}$ and ϕIRS-$2^{-/-}$ mice at 12 weeks after transplantation. The mRNA expression was determined by quantitative RT-PCR. The gene expression is expressed relative to the respective level of expression in those of ϕIRS-$2^{+/+}$ mice, which was set at 1.0 ($n = 4$ each). (D) Peritoneal macrophages isolated from ϕIRS-$2^{+/+}$ mice and ϕIRS-$2^{-/-}$ mice were harvested at 12 weeks after transplantation. The mRNA expression was determined by quantitative RT-PCR ($n = 3$ each). (E) MCP-1-positive monocytes/macrophages adherent to endothelial cells were visualized by double immunostaining with Mac-2 and MCP-1 antibodies under a confocal laser scanning microscope at 12 weeks after transplantation (upper panel). Percentage of MCP-1-positive cells per all Mac-2-positive cells adherent to the endothelial cells ($n = 7$) (lower panel). All data are expressed as mean ± SEM. $^*P < 0.05$ vs. ϕIRS-$2^{+/+}$ mice.

3.3. IRS-2 deficiency in macrophages enhances macrophage adhesion to endothelium in LPS-treated mice

In order to evaluate the effect of IRS-2 deficiency in macrophages on their adhesion to the endothelium induced by acute inflammation, ϕIRS-$2^{-/-}$ and ϕIRS-$2^{+/+}$ mice on normal chow diet were injected with LPS (1 mg/kg) at 8 weeks after bone marrow transplantation. Although both groups of LPS-treated mice exhibited significant increases in macrophage adhesion to the endothelium at 6 h after LPS injection (Fig. 4), the induction of macrophage adhesion was more significant in ϕIRS-$2^{-/-}$ mice than ϕIRS-$2^{+/+}$.

4. Discussion

The present study demonstrated that IRS-2 deficiency in macrophages increased macrophage accumulation in the vascular wall independent of the metabolic changes including lipid profile. In addition, the reduced IRS-2-mediated insulin signal in macrophages impaired the suppression of proinflammatory mediators in macrophages, which may contribute to the above phenotype.

The present study demonstrated that IRS-2 deficiency in macrophages was associated with increased MCP-1 expression. The atherogenic effects of MCP-1 are firmly established. Indeed,

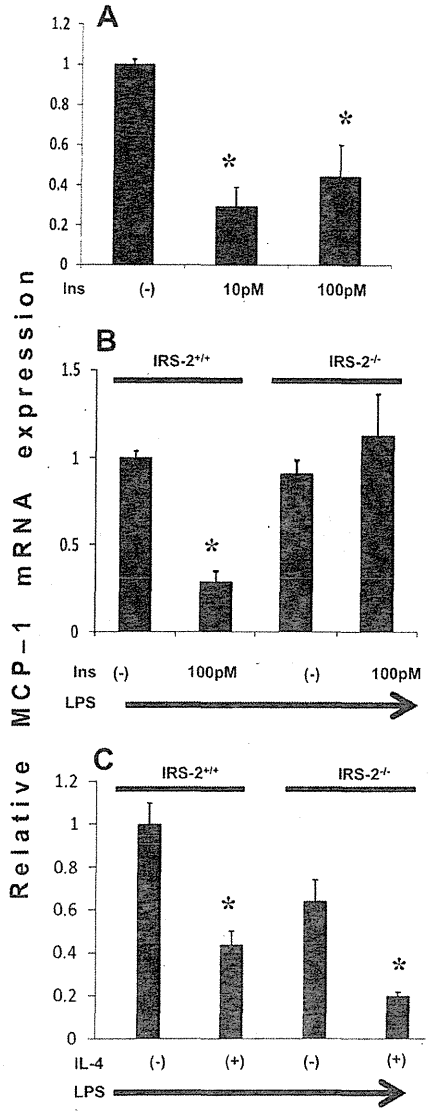

Fig. 3. IRS-2 stimulated by physiological concentration of insulin suppresses MCP-1 expression. (A) Peritoneal macrophages isolated from C57BL/6 mice were incubated with physiological concentrations of insulin (10 and 100 pM) for 6 h. Then, macrophages were used for isolation of total RNA. The mRNA expression was determined by quantitative RT-PCR. The MCP-1 gene expression is expressed relative to the level of expression in peritoneal macrophages without the addition of insulin, which was set at 1.0 ($n = 4$, respectively). $^*P < 0.05$ vs. without insulin. (B) *Peritoneal macrophages isolated from* ϕIRS-$2^{+/+}$ *mice and* ϕIRS-$2^{-/-}$ *mice at* 8 weeks after transplantation were used for isolation of total RNA. The MCP-1 gene expression is expressed relative to that of ϕIRS-$2^{+/+}$ mice without insulin treatment, which was set at 1.0 ($n = 3$–4). $^*P < 0.05$ vs. ϕIRS-$2^{+/+}$ mice. (C) Peritoneal macrophages isolated from ϕIRS-$2^{+/+}$ and ϕIRS-$2^{-/-}$ mice at 8 weeks after transplantation were used for isolation of total RNA. The MCP-1 gene expression is expressed relative to that of ϕIRS-$2^{+/+}$ mice without IL-4 treatment, which was set at 1.0 ($n = 3$–4). $^*P < 0.05$ vs. without IL-4. Data represent the mean ± SEM values.

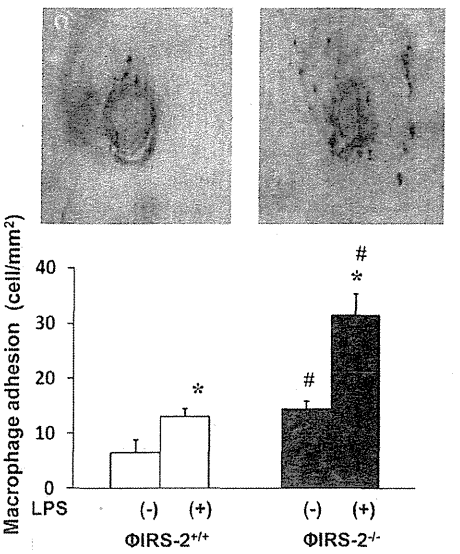

Fig. 4. Enhanced macrophage adhesion to the endothelium in ϕIRS-$2^{-/-}$ mice during acute inflammatory reaction. At 6 h after intraperitoneal injection of LPS (1 mg/kg) into ϕIRS-$2^{+/+}$ and ϕIRS-$2^{-/-}$ mice, *en face* immunohistochemical staining of thoracic aorta was performed with Mac2 antibody. Representative *en face* views of immunohistochemical staining with Mac2 antibody in thoracic aorta in ϕIRS-$2^{+/+}$ and ϕIRS-$2^{-/-}$ mice (upper panel). The density of adherent Mac2-positive cells on endothelial cells at branching areas ($n = 5$). Data are expressed as mean ± SEM. $^*P < 0.05$ vs. ϕIRS-$2^{+/+}$ mice or ϕIRS-$2^{-/-}$ mice without LPS. $\#P < 0.05$ vs. ϕIRS-$2^{+/+}$ with or without LPS.

MCP-1-deficient mice have markedly reduced atherosclerotic lesions [24]. Furthermore, forced expression of MCP-1 in leukocytes is known to induce advanced atherosclerotic lesions [25]. Thus, overexpression of this inflammatory mediator in activated macrophages may play a causal role in macrophage accumulation in the vascular wall.

It was reported that reduced insulin signal pathways, both of IRS2/PI3K/Akt and IRS2/Erk, result in overexpression of MCP-1 mRNA in macrophages and that apoE$^{-/-}$ IRS-$2^{+/-}$ mice show enhanced atherosclerogenesis [17]. In the present study, we also demonstrated that exposure of macrophages to physiological concentrations of insulin suppressed the expression of MCP-1. Other studies showed that insulin receptor$^{-/-}$ macrophages enhance the expression of inflammatory genes at the basal state [10,16] and that LDL receptor$^{-/-}$ mice transplanted with insulin receptor$^{-/-}$ bone marrow develop larger atherosclerotic lesions accompanied by a pronounced increase in apoptotic cells and necrotic core formation [9]. The present study demonstrated enhanced monocyte adhesion to the arterial wall and their invasion of the arterial wall in ϕIRS-$2^{-/-}$ mice even in the absence of any metabolic abnormality including lipid profile. These findings suggest that physiological insulin signal protects against atherosclerogenesis.

On the other hand, a previous study showed that high dose of insulin up-regulated the expression of TNF-α mRNA in THP-1 macrophages [26]. This finding suggests that hyperinsulinemia may potentially enhance the progression of atherosclerosis through its effect on macrophages, similar to that on endothelial cells [27] and on vascular smooth muscle cells [28]. It has been demonstrated that 24-h exposure to high-dose insulin downregulates insulin receptor protein expression in macrophages and contributes to atherosclerotic changes [8]. Considered together, our results and those of others suggest that insulin may have beneficial as well as potentially harmful effects on the progression of atherosclerosis through the expression of proinflammatory mediators. This effect seems to depend on its concentration, similar to endothelial cells [3,4,27].

The present results showed that deficiency of IRS-2 in macrophages enhanced macrophage accumulation in the vascular wall under not only normal diet condition, but also LPS-induced acute inflammatory condition. In contrast to our data, ApoE$^{-/-}$ mice transplanted with IRS2$^{-/-}$ bone marrow exhibited milder atherosclerosis at more advanced stage under extreme hypercholesterolemic conditions [10]. The exact reasons for the differences are not completely clear at present. However, since atherosclerosis is a

complex pathological process, it is possible that the reduced IRS-2-mediated signal in macrophages could exert a different effect on each step of atherosclerosis.

In conclusion, we provided evidence that the reduced IRS-2-mediated insulin signal in macrophages enhances macrophage accumulation in the vascular wall accompanied by increased expression of proinflammatory mediators. These data suggest that reduced IRS-2-mediated insulin signal in macrophages is a potentially important therapeutic target to prevent the progression of atherosclerosis in patients with type 2 diabetes.

Duality of interest

The authors declare no duality of interest in relation to this manuscript.

Acknowledgments

The authors thank Mrs. Naoko Daimaru, Eriko Magoshi, and Kiyomi Nakamura for the excellent technical assistance. This work was supported by grants from the Ministry of Education, Sports and Culture of Japan, and Suzuken Memorial Foundation.

References

[1] J.P. Despres, B. Lamarche, P. Mauriege, B. Cantin, G.R. Dagenais, S. Moorjani, P.J. Lupien, Hyperinsulinemia as an independent risk factor for ischemic heart disease, N. Engl. J. Med. 334 (1996) 952–957.
[2] J. Nigro, N. Osman, A.M. Dart, P.J. Little, Insulin resistance and atherosclerosis, Endocr. Rev. 27 (2006) 242–259.
[3] D. Vicent, J. Ilany, T. Kondo, K. Naruse, S.J. Fisher, Y.Y. Kisanuki, S. Bursell, M. Yanagisawa, G.L. King, C.R. Kahn, The role of endothelial insulin signaling in the regulation of vascular tone and insulin resistance, J. Clin. Invest. 111 (2003) 1373–1380.
[4] E.R. Duncan, P.A. Crossey, S. Walker, N. Anilkumar, L. Poston, G. Douglas, V.A. Ezzat, S.B. Wheatcroft, A.M. Shah, M.T. Kearney, Effect of endothelium-specific insulin resistance on endothelial function in vivo, Diabetes 57 (2008) 3307–3314.
[5] T. Kubota, N. Kubota, M. Moroi, Y. Terauchi, T. Kobayashi, K. Kamata, R. Suzuki, K. Tobe, A. Namiki, S. Aizawa, R. Nagai, T. Kadowaki, T. Yamaguchi, Lack of insulin receptor substrate-2 causes progressive neointima formation in response to vessel injury, Circulation 107 (2003) 3073–3080.
[6] C.P. Liang, S. Han, T. Senokuchi, A.R. Tall, The macrophage at the crossroads of insulin resistance and atherosclerosis, Circ. Res. 100 (2007) 1546–1555.
[7] T. Mita, H. Goto, K. Azuma, W.L. Jin, T. Nomiyama, Y. Fujitani, T. Hirose, R. Kawamori, H. Watada, Impact of insulin resistance on enhanced monocyte adhesion to endothelial cells and atherosclerogenesis independent of LDL cholesterol level, Biochem. Biophys. Res. Commun. 395 (2010) 477–483.
[8] C.P. Liang, S. Han, H. Okamoto, R. Carnemolla, I. Tabas, D. Accili, A.R. Tall, Increased CD36 protein as a response to defective insulin signaling in macrophages, J. Clin. Invest. 113 (2004) 764–773.
[9] S. Han, C.P. Liang, T. DeVries-Seimon, M. Ranalletta, C.L. Welch, K. Collins-Fletcher, D. Accili, I. Tabas, A.R. Tall, Macrophage insulin receptor deficiency increases ER stress-induced apoptosis and necrotic core formation in advanced atherosclerotic lesions, Cell. Metab. 3 (2006) 257–266.
[10] J. Baumgartl, S. Baudler, M. Scherner, V. Babaev, L. Makowski, J. Suttles, M. McDuffie, K. Tobe, T. Kadowaki, S. Fazio, C.R. Kahn, G.S. Hotamisligil, W. Krone, M. Linton, J.C. Bruning, Myeloid lineage cell-restricted insulin resistance protects apolipoprotein E-deficient mice against atherosclerosis, Cell Metab. 3 (2006) 247–256.
[11] J.C. O'Connor, C.L. Sherry, C.B. Guest, G.G. Freund, Type 2 diabetes impairs insulin receptor substrate-2-mediated phosphatidylinositol 3-kinase activity in primary macrophages to induce a state of cytokine resistance to IL-4 in association with overexpression of suppressor of cytokine signaling-3, J. Immunol. 178 (2007) 6886–6893.
[12] A. Aljada, H. Ghanim, R. Saadeh, P. Dandona, Insulin inhibits NFkappaB and MCP-1 expression in human aortic endothelial cells, J. Clin. Endocrinol. Metab. 86 (2001) 450–453.
[13] P. Dandona, A. Aljada, P. Mohanty, H. Ghanim, W. Hamouda, E. Assian, S. Ahmad, Insulin inhibits intranuclear nuclear factor kappaB and stimulates IkappaB in mononuclear cells in obese subjects: evidence for an anti-inflammatory effect? J. Clin. Endocrinol. Metab. 86 (2001) 3257–3265.
[14] J.O. Martins, M. Ferracini, N. Ravanelli, R.G. Landgraf, S. Jancar, Insulin inhibits LPS-induced signaling pathways in alveolar macrophages, Cell Physiol. Biochem. 21 (2008) 297–304.
[15] D. Su, G.M. Coudriet, D. Hyun Kim, Y. Lu, G. Perdomo, S. Qu, S. Slusher, H.M. Tse, J. Piganelli, N. Giannoukakis, J. Zhang, H. Henry Dong, FoxO1 links insulin resistance to proinflammatory cytokine IL-1beta production in macrophages, Diabetes 58 (2009) 2624–2633.
[16] T. Senokuchi, C.P. Liang, T.A. Seimon, S. Han, M. Matsumoto, A.S. Banks, J.H. Paik, R.A. DePinho, D. Accili, I. Tabas, A.R. Tall, Forkhead transcription factors (FoxOs) promote apoptosis of insulin-resistant macrophages during cholesterol-induced endoplasmic reticulum stress, Diabetes 57 (2008) 2967–2976.
[17] H. Gonzalez-Navarro, A. Vinue, M. Vila-Caballer, A. Fortuno, O. Beloqui, G. Zalba, D. Burks, J. Diez, V. Andres, Molecular mechanisms of atherosclerosis in metabolic syndrome: role of reduced IRS2-dependent signaling, Arterioscler. Thromb. Vasc. Biol. 28 (2008) 2187–2194.
[18] N. Kubota, K. Tobe, Y. Terauchi, K. Eto, T. Yamauchi, R. Suzuki, Y. Tsubamoto, K. Komeda, R. Nakano, H. Miki, S. Satoh, H. Sekihara, S. Sciacchitano, M. Lesniak, S. Aizawa, R. Nagai, S. Kimura, Y. Akanuma, S.I. Taylor, T. Kadowaki, Disruption of insulin receptor substrate 2 causes type 2 diabetes because of liver insulin resistance and lack of compensatory beta-cell hyperplasia, Diabetes 49 (2000) 1880–1889.
[19] H. Yamada, M. Yoshida, Y. Nakano, T. Suganami, N. Satoh, T. Mita, K. Azuma, M. Itoh, Y. Yamamoto, Y. Kamei, M. Horie, H. Watada, Y. Ogawa, In vivo and in vitro inhibition of monocyte adhesion to endothelial cells and endothelial adhesion molecules by eicosapentaenoic acid, Arterioscler. Thromb. Vasc. Biol. 28 (2008) 2173–2179.
[20] J.B. Choi, H. Uchino, K. Azuma, N. Iwashita, Y. Tanaka, H. Mochizuki, M. Migita, T. Shimada, R. Kawamori, H. Watada, Little evidence of transdifferentiation of bone marrow-derived cells into pancreatic beta cells, Diabetologia 46 (2003) 1366–1374.
[21] S. Nakayama, T. Uchida, J.B. Choi, Y. Fujitani, T. Ogihara, N. Iwashita, K. Azuma, H. Mochizuki, T. Hirose, R. Kawamori, M. Inoue, H. Watada, Impact of whole body irradiation and vascular endothelial growth factor-A on increased beta cell mass after bone marrow transplantation in a mouse model of diabetes induced by streptozotocin, Diabetologia 52 (2009) 115–124.
[22] T. Mita, A. Otsuka, K. Azuma, T. Uchida, T. Ogihara, Y. Fujitani, T. Hirose, M. Mitsumata, R. Kawamori, H. Watada, Swings in blood glucose levels accelerate atherogenesis in apolipoprotein E-deficient mice, Biochem. Biophys. Res. Commun. 358 (2007) 679–685.
[23] M. Arakawa, T. Mita, K. Azuma, C. Ebato, H. Goto, T. Nomiyama, Y. Fujitani, T. Hirose, R. Kawamori, H. Watada, Inhibition of monocyte adhesion to endothelial cells and attenuation of atherosclerotic lesion by a glucagon-like peptide-1 receptor agonist, exendin-4, Diabetes 59 (2010) 1030–1037.
[24] L. Gu, Y. Okada, S.K. Clinton, C. Gerard, G.K. Sukhova, P. Libby, B.J. Rollins, Absence of monocyte chemoattractant protein-1 reduces atherosclerosis in low density lipoprotein receptor-deficient mice, Mol. Cell 2 (1998) 275–281.
[25] R.J. Aiello, P.A. Bourassa, S. Lindsey, W. Weng, E. Natoli, B.J. Rollins, P.M. Milos, Monocyte chemoattractant protein-1 accelerates atherosclerosis in apolipoprotein E-deficient mice, Arterioscler. Thromb. Vasc. Biol. 19 (1999) 1518–2155.
[26] K.T. Iida, H. Shimano, Y. Kawakami, H. Sone, H. Toyoshima, S. Suzuki, T. Asano, Y. Okuda, N. Yamada, Insulin up-regulates tumor necrosis factor-alpha production in macrophages through an extracellular-regulated kinase-dependent pathway, J. Biol. Chem. 276 (2001) 32531–32537.
[27] D.J. Schneider, P.M. Absher, M.A. Ricci, Dependence of augmentation of arterial endothelial cell expression of plasminogen activator inhibitor type 1 by insulin on soluble factors released from vascular smooth muscle cells, Circulation 96 (1997) 2868–2876.
[28] C.C. Wang, I. Gurevich, B. Draznin, Insulin affects vascular smooth muscle cell phenotype and migration via distinct signaling pathways, Diabetes 52 (2003) 2562–2569.

Published November 14, 2011

JEM

Article

Evi1 is essential for hematopoietic stem cell self-renewal, and its expression marks hematopoietic cells with long-term multilineage repopulating activity

Keisuke Kataoka,[1] Tomohiko Sato,[1] Akihide Yoshimi,[1] Susumu Goyama,[1] Takako Tsuruta,[1] Hiroshi Kobayashi,[1] Munetake Shimabe,[1] Shunya Arai,[1] Masahiro Nakagawa,[1] Yoichi Imai,[1] Keiki Kumano,[1] Katsuyoshi Kumagai,[2] Naoto Kubota,[2] Takashi Kadowaki,[2] and Mineo Kurokawa[1]

[1]Department of Hematology and Oncology, [2]Department of Diabetes and Metabolic Diseases, Graduate School of Medicine, University of Tokyo, Bunkyo-ku, Tokyo, 113-8655, Japan

Ecotropic viral integration site 1 (Evi1), a transcription factor of the SET/PR domain protein family, is essential for the maintenance of hematopoietic stem cells (HSCs) in mice and is overexpressed in several myeloid malignancies. Here, we generate reporter mice in which an internal ribosome entry site (IRES)-GFP cassette is knocked-in to the *Evi1* locus. Using these mice, we find that Evi1 is predominantly expressed in long-term HSCs (LT-HSCs) in adult bone marrow, and in the hematopoietic stem/progenitor fraction in the aorta-gonad-mesonephros, placenta, and fetal liver of embryos. In both fetal and adult hematopoietic systems, Evi1 expression marks cells with long-term multilineage repopulating activity. When combined with conventional HSC surface markers, sorting according to Evi1 expression markedly enhances purification of cells with HSC activity. Evi1 heterozygosity leads to marked impairment of the self-renewal capacity of LT-HSCs, whereas overexpression of Evi1 suppresses differentiation and boosts self-renewal activity. Reintroduction of Evi1, but not Mds1-Evi1, rescues the HSC defects caused by Evi1 heterozygosity. Thus, in addition to documenting a specific relationship between Evi1 expression and HSC self-renewal activity, these findings highlight the utility of Evi1-IRES-GFP reporter mice for the identification and sorting of functional HSCs.

CORRESPONDENCE
Mineo Kurokawa:
kurokawa-tky@umin.ac.jp

Abbreviations used: AGM, aorta-gonad-mesonephros; AML, acute myeloid leukemia; BFU-E, burst-forming unit-erythrocyte; CFU-S, CFU-spleen; CLP, common lymphoid progenitor; CMP, common myeloid progenitor; CRA, competitive repopulation assay; EC, endothelial cell; ES, embryonic stem; Evi1, ecotropic viral integration site 1; FL, fetal liver; GEMM, granulocyte/erythrocyte/ macrophage/megakaryocyte; GM, granulocyte/macrophage; GMP, GM progenitor; HSC, hematopoietic stem cell; HSPC, hematopoietic stem/progenitor cell; IRES, internal ribosome entry site; Lin, lineage; LSK, Lin$^-$ Sca-1$^+$ c-kit$^+$; LT-HSC, long-term HSC; ME, Mds1-Evi1; MEP, megakaryocyte/erythrocyte progenitor; MPP, multipotent progenitor; MSC, mesenchymal stem cell; MSL, Mac-1$^+$ Sca-1$^+$ Lin$^-$; OB, osteoblast; pA, polyadenylation; PB, peripheral blood; RQ-PCR, real-time quantitative PCR; SCF, stem cell factor; ST-HSC, short-term HSC; TPO, thrombopoietin.

Hematopoietic stem cells (HSCs) are distinguished by their inherent capacity to perpetuate themselves through self-renewal and to generate multiple blood cell lineages through differentiation. To maintain a steady-state pool of self-renewing HSCs and prevent HSC exhaustion, these defining properties of HSCs must be tightly regulated. Fine-tuning of stem cell properties requires stem cell–specific expression of their regulatory genes. To elucidate the stemness transcriptional profile, several gene expression microarray analyses have identified quite a few number of HSC-specific gene candidates (Ramalho-Santos et al., 2002; Akashi et al., 2003; Forsberg et al., 2010). However, most of the molecules established to be associated with the regulation of self-renewal capacity in HSCs are widely expressed in the hematopoietic system, and their mutations in genetic models are exclusively accompanied with other hematological abnormalities. Thus, a bona fide stem cell–specific regulator of their function has not been identified, and the functional identification of HSCs based on their ability to self-renew remains difficult.

Ecotropic viral integration site 1 (Evi1) is an oncogenic transcription factor that belongs to the SET/PR domain protein family (Goyama and Kurokawa, 2009). We and others have reported that Evi1 accomplishes an important regulatory function in hematopoietic stem/progenitor

K. Kataoka and T. Sato contributed equally to this paper.

The Rockefeller University Press $30.00
J. Exp. Med. Vol. 208 No. 12 2403-2416
www.jem.org/cgi/doi/10.1084/jem.20110447

Published November 14, 2011

cells (HSPCs) during fetal and adult development. Evi1 expression is limited to HSPCs in the embryonic and adult hematopoietic systems. HSCs in *Evi1*$^{-/-}$ embryos are markedly decreased in numbers with defective repopulating capacity (Yuasa et al., 2005). Moreover, conditional deletion of Evi1 in adult mice revealed that Evi1 is essential for the maintenance of HSCs, but is dispensable for lineage commitment (Goyama et al., 2008). Besides the importance of Evi1 in normal hematopoiesis, dysregulation of Evi1 expression can have distinct oncogenic potential in various myeloid malignancies (Goyama and Kurokawa, 2009). Indeed, aberrant EVI1 expression defines a unique subset of acute myeloid leukemia (AML), and predicts adverse outcome in patients (Lugthart et al., 2008; Gröschel et al., 2010). Furthermore, Evi1 overexpression in hematopoietic cells leads to myelodysplasia in a murine BM transplant model (Buonamici et al., 2004).

In this study, using newly generated Evi1-GFP reporter mice, we demonstrate that Evi1 is preferentially expressed in LT-HSCs, and its expression can mark in vivo long-term multilineage repopulating HSCs and improve the conventional HSC isolation strategy in both adult BM and embryo, which suggests a distinctive relationship between Evi1 and HSC function. Consistent with this, heterozygosity of Evi1 causes a striking reduction in the number of LT-HSCs, with a specific defect of self-renewal capacity caused by accelerated differentiation. Our results point to a potential utility of an Evi1-GFP reporter mouse line for the functional identification of HSCs based on their self-renewal activity, and a central role of Evi1 in regulating the homeostasis of HSCs.

RESULTS

Evi1 is predominantly expressed in LT-HSCs in adult BM

To elucidate Evi1 expression within the hematopoietic system, we have generated gene-targeted mice in which an internal ribosome entry site (IRES)-GFP cassette is knocked-in to the *Evi1* locus by homologous recombination (Fig. 1 A). This knock-in allele functions in a bicistronic manner in that expression of both Evi1 and GFP is under the endogenous transcriptional regulatory elements of the *Evi1* gene, thus enabling us to track Evi1 expression on an individual cell basis. Appropriately targeted TT2 embryonic stem (ES) cell clones were identified by Southern blotting (Fig. 1 B). Mice heterozygous for the *Evi1-IRES-GFP* allele (*Evi1*$^{+/GFP}$) were distinguished from WT mice by genotyping PCR (Fig. 1 C). Western blot analysis showed the presence of GFP protein and comparable expression of Evi1 protein in embryonic fibroblast cells from *Evi1*$^{+/GFP}$ mice compared with WT mice (Fig. 1 D). *Evi1*$^{+/GFP}$ mice were phenotypically indistinguishable in survival, hematopoietic cellularity, and lineage composition from WT controls (unpublished data). Initial flow cytometric analysis of adult *Evi1*$^{+/GFP}$ mice revealed a small, but discrete, population of GFP$^+$ cells (0.15 ± 0.6%; Fig. 2 A), confirming the expression of the *Evi1-IRES-GFP* allele. To examine whether GFP expression levels correlated with those of endogenous *Evi1* mRNA expression, *Evi1* expression of sorted GFP$^-$ and GFP$^+$ cells from BM of *Evi1*$^{+/GFP}$ mice was analyzed by real-time quantitative PCR (RQ-PCR). *Evi1* mRNA was exclusively expressed in the GFP$^+$ cells, and almost no expression was found in the GFP$^-$ cells (Fig. 2 B), indicating that GFP expression in this mouse model faithfully marks cells with active Evi1 expression.

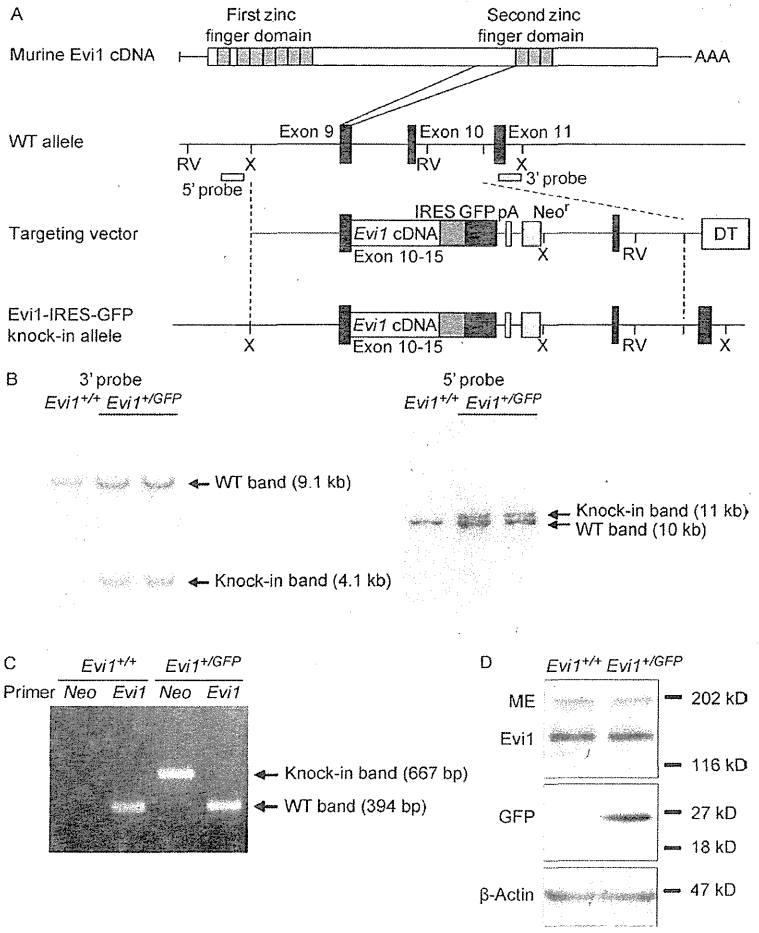

Figure 1. Generation of Evi1-IRES-GFP knock-in mice. (A) The structure of murine *Evi1* and the targeted *Evi1-IRES-GFP* locus is shown. RV, EcoRV; X, XbaI. (B) Southern blot analysis of genomic DNA isolated from WT ES cells (*Evi1*$^{+/+}$) and two independent clones of targeted ES cells (*Evi1*$^{+/GFP}$). DNA was digested with XbaI (left) or EcoRV (right), and hybridized with the indicated probes. (C) Genotyping of *Evi1*$^{+/GFP}$ mice by PCR. (D) Western blot analysis for GFP and Evi1 in embryonic fibroblast cells from *Evi1*$^{+/+}$ and *Evi1*$^{+/GFP}$ mice. β-Actin was used as a loading control. ME, Mds1-Evi1.

Published November 14, 2011

Evi1 mRNA has been shown to be expressed at significantly higher levels in HSPCs (Lin$^-$ Sca-1$^+$ c-kit$^+$ [LSK]) and common lymphoid progenitors (CLPs) than in other hematopoietic cells (Yuasa et al., 2005; Chen et al., 2008). To gain insight into the biological function of Evi1 through its cell type–specific expression pattern, the distribution of GFP$^+$ cells was examined in adult BM from *Evi1*$^{+/GFP}$ mice. Beyond expectation, GFP expression was highly restricted to the LSK fraction (Fig. 2 A). To confirm stem/progenitor-specific expression of Evi1, we analyzed the GFP fluorescence of various hematopoietic cell populations from BM and spleen of *Evi1*$^{+/GFP}$ mice. We found a heterogeneous expression of GFP in the LSK fraction, in which about half of the cells were GFP$^+$ (Fig. 2, C and D). Conversely, only 2.5% of common myeloid progenitors (CMPs) expressed GFP, and almost no expression was found in granulocyte/monocyte progenitors (GMPs) and megakaryocyte/erythrocyte progenitors (MEPs; Fig. 2 C). In contrast to the previous study (Chen et al., 2008), GFP was not expressed in CLPs (Fig. 2 C). In addition, no GFP expression was observed in mature hematopoietic lineages or nonhematopoietic cells in BM (Fig. 2 C). Together, these results suggest that Evi1 is uniquely expressed in HSPCs, but its expression is sharply down-regulated along with differentiation.

Because LSK cells, a population which contains multipotent progenitors (MPPs), short-term HSCs (ST-HSCs), and long-term HSCs (LT-HSCs), include both a GFP$^+$ fraction and a GFP$^-$ fraction, we next resolved GFP expression within the LSK compartment for other markers characteristic of LT-HSCs. When LSK cells were subdivided according to CD34 and Flk-2 expression (Orford and Scadden, 2008), the Flk-2$^-$ CD34$^-$ LSK fraction, which is considered to contain most LT-HSC activity, had the highest expression of GFP, and its expression decreased with differentiation to hematopoietic progenitors (Fig. 2 E). In addition, further enrichment for LT-HSCs within the LSK fraction using SLAM family receptors (CD48 and CD150; Kiel et al., 2005) revealed that GFP$^+$ cells were found in greatest abundance within CD48$^-$ CD150$^+$ LSK cells, in which LT-HSCs are highly enriched. In contrast, GFP expression was substantially down-regulated in CD48$^+$ LSK cells, irrespective of CD150 expression (Fig. 2 F). When we examined how GFP$^+$ cells were distributed within the LSK fraction, GFP expression was highly enriched in the Flk-2$^-$ CD34$^-$ LSK or CD48$^-$ CD150$^+$ LSK fractions (Fig. 2, G and H). Therefore, these results indicate that Evi1 is dynamically regulated within HSPCs; its

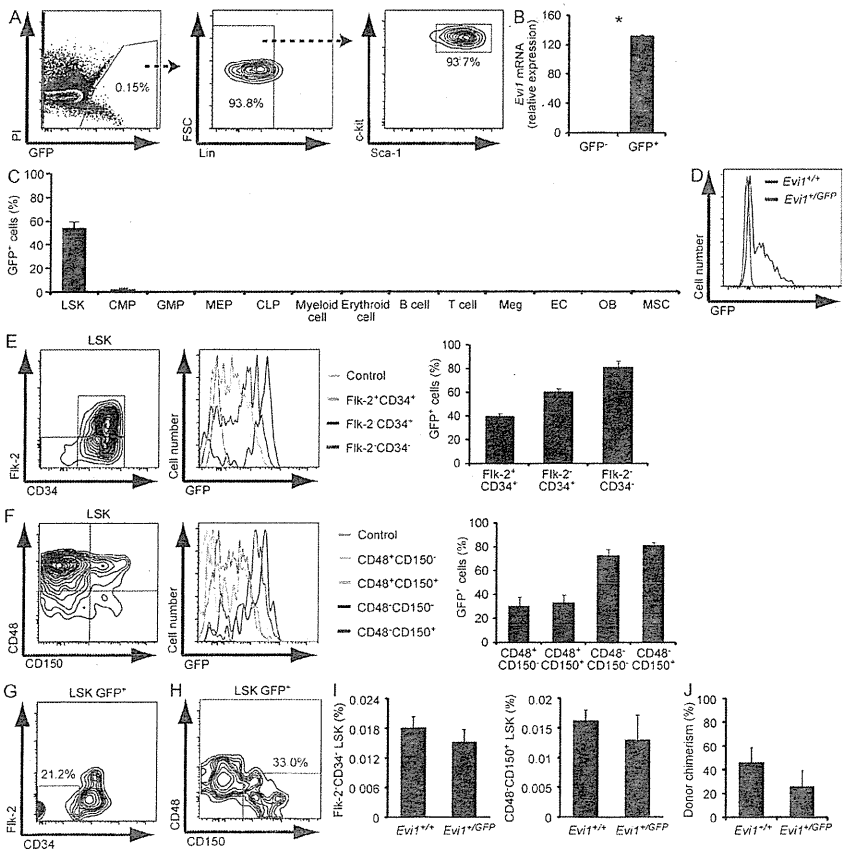

Figure 2. Evi1 is predominantly expressed in LT-HSCs in adult BM. (A) FACS analysis of expression of lineage markers (Lin), c-kit, and Sca-1 on GFP$^+$ cells in adult BM from *Evi1*$^{+/GFP}$ mice. Data are representative of three independent experiments. PI, propidium iodide; FSC, forward scatter. (B) RQ-PCR analysis of the expression of *Evi1* mRNA in sorted GFP$^-$ or GFP$^+$ cells from BM of *Evi1*$^{+/GFP}$ mice, presented relative to GAPDH expression (*, $P < 0.0001$; $n = 2$). (C) Frequency of GFP$^+$ cells in indicated BM subpopulation and in splenic T cells from *Evi1*$^{+/GFP}$ mice ($n = 3$–5). Meg, megakaryocyte; EC, endothelial cell. (D) FACS analysis of expression of GFP in LSK cells from *Evi1*$^{+/+}$ and *Evi1*$^{+/GFP}$ mice. Data are representative of at least twenty independent experiments. (E and F) Frequency of GFP$^+$ cells in subpopulations of LSK cells divided using Flk-2 and CD34 (E) or CD48 and CD150 (F) in *Evi1*$^{+/GFP}$ mice. (left) Representative plot is shown. (right) Bar graph represents mean ± SD ($n = 3$–4). (G–H) FACS analysis of expression of Flk-2 and CD34 (G) or CD48 and CD150 (H) on LSK GFP$^+$ cells in BM from *Evi1*$^{+/GFP}$ mice. Data are representative of two independent experiments. (I) Frequency of Flk-2$^-$ CD34$^-$ LSK or CD48$^-$ CD150$^+$ LSK cells in BM from *Evi1*$^{+/+}$ and *Evi1*$^{+/GFP}$ mice ($n = 3$–5). (J) PB donor chimerism in CRAs, in which 2 × 10^5 BM cells from *Evi1*$^{+/+}$ and *Evi1*$^{+/GFP}$ mice (Ly5.1) were transplanted into lethally irradiated recipients (Ly5.2) together with 2 × 10^5 competitor BM cells (Ly5.2). Percentages of donor-derived cells (Ly5.1) in PB 16 wk after transplantation are shown ($P = 0.12$; $n = 3$). Data represent mean ± SD.

Published November 14, 2011

expression is predominantly enriched in LT-HSCs and rapidly extinguished during early stages of lineage commitment.

To reinforce Evi1-IRES-GFP knock-in mice as a faithful tool for investigating HSCs, we assessed the number and function of LT-HSCs in BM from *Evi1*$^{+/GFP}$ mice. Flow cytometric analysis revealed that the frequencies of Flk-2$^-$ CD34$^-$ LSK or CD48$^-$ CD150$^+$ LSK cells were comparable between *Evi1*$^{+/+}$ and *Evi1*$^{+/GFP}$ mice (Fig. 2 I). In addition, a competitive repopulation assay (CRA) showed that *Evi1*$^{+/GFP}$ BM cells exhibited slightly less, but not significantly different, long-term reconstitution capacity (Fig. 2 J), indicating that the number and function of HSCs in *Evi1*$^{+/GFP}$ mice are similar to WT controls.

Evi1 expression represents a functionally distinct population that remains in an undifferentiated and quiescent state within HSPCs

As only a subset of LSK cells expressed GFP in *Evi1*$^{+/GFP}$ mice, we hypothesized that Evi1 expression functionally divides the LSK population and marks a more undifferentiated and quiescent state with multipotent differentiation properties in this population. To test this idea, we separated the LSK population into LSK GFP$^-$ and LSK GFP$^+$ cells and compared their biological functions. Initially, we confirmed that LSK GFP$^+$ cells had a much higher level of *Evi1* transcripts than LSK GFP$^-$ cells by RQ-PCR analysis (Fig. 3 A). Interestingly, despite the negative GFP expression, LSK GFP$^-$ cells expressed *Evi1* mRNA at a higher level compared with CMPs and GMPs (Fig. 3 A), which also suggests that Evi1 expression is inversely proportional to the differentiation status. To achieve an estimate of the differentiation stage of these two populations, LSK GFP$^-$ and LSK GFP$^+$ cells were cultured in serum-free medium containing stem cell factor (SCF) and thrombopoietin (TPO). After 3 d of culture, the proportion that remained in the LSK fraction was significantly higher in LSK GFP$^+$ cells than in LSK GFP$^-$ cells (Fig. 3 B), suggesting that LSK GFP$^+$ cells are more primitive HSCs. Next, to evaluate the differentiation potential of LSK GFP$^-$ and LSK GFP$^+$ cells, we performed colony-forming assays in vitro. Although both populations generated an equivalent number of myeloid colonies CFU-granulocyte/macrophage [CFU-GM]), LSK GFP$^+$ cells gave rise to greater numbers of erythroid (burst-forming unit-erythrocyte [BFU-E]) and multipotential (CFU-granulocyte/erythrocyte/macrophage/megakaryocyte [CFU-GEMM]) colonies than LSK GFP$^-$ cells (Fig. 3 C). These data suggest that Evi1 expression correlates with multipotent differentiation capacity. In addition, to assess the colony-forming capacity at the clonal level, single LSK GFP$^-$ and LSK GFP$^+$ cells were cultured in serum-free medium. LSK GFP$^-$ cells formed detectable colonies at a frequency comparable to LSK GFP$^+$ cells, but generated smaller numbers of highly proliferative colonies (>300 cells; Fig. 3 D), indicating that the LSK GFP$^+$ fraction comprises a higher proportion of HSPCs with enhanced proliferative capacity.

Our observations suggested that Evi1 reporter activity is down-regulated as HSCs differentiate. To examine this issue, we forced LSK GFP$^+$ cells to differentiate in vitro in response to SCF, TPO, IL-3, and IL-6. These LSK GFP$^+$ cells predominantly generated GFP$^-$ cells (Fig. 3 E). After culture, the majority of cells that had become GFP$^-$ lost the LSK phenotype, whereas most cells that remained in GFP$^+$ continued to express

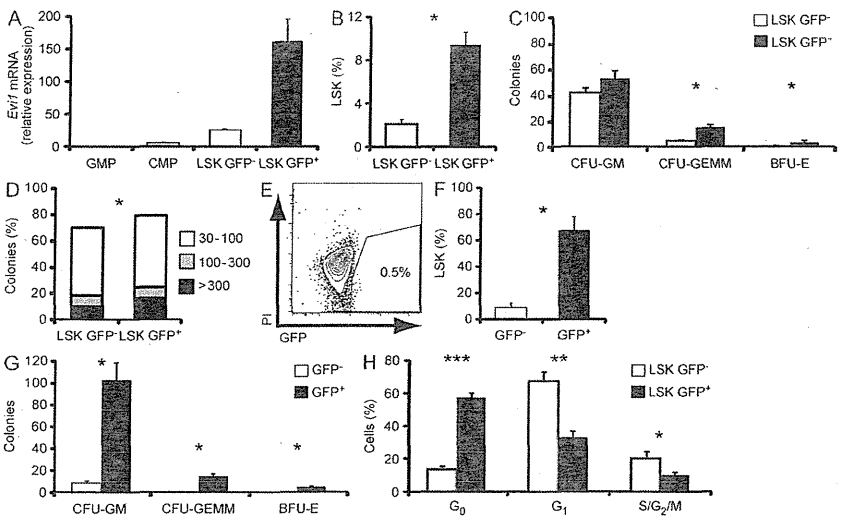

Figure 3. Evi1 expression represents a functionally distinct population that remains in an undifferentiated and quiescent state within HSPCs. (A) RQ-PCR analysis of the expression of *Evi1* mRNA in sorted GMPs, CMPs, LSK GFP$^-$ cells, and LSK GFP$^+$ cells from *Evi1*$^{+/GFP}$ mice, presented relative to *GAPDH* expression ($n = 2$). (B) LSK GFP$^-$ and LSK GFP$^+$ cells were cultured in serum-free medium with 20 ng/ml SCF and 20 ng/ml TPO for 3 d, and the percentage of the remaining LSK fraction was analyzed (*, $P < 0.001$; $n = 3$). (C) Numbers of CFU-GM, CFU-GEMM, and BFU-E colonies derived from 100 sorted LSK GFP$^-$ and LSK GFP$^+$ cells (*, $P < 0.05$; $n = 3$). (D) Single LSK GFP$^-$ and LSK GFP$^+$ cells from *Evi1*$^{+/GFP}$ mice were clone-sorted and cultured in serum-free medium. After 14 d of culture, cell numbers in each colony were analyzed. Their relative distribution is shown (*, $P < 0.05$; $n = 192$ clones from 2 independent experiments). (E) LSK GFP$^+$ cells were cultured in medium containing 10% serum with 50 ng/ml SCF, 50 ng/ml TPO, 10 ng/ml IL-3, and 10 ng/ml IL-6 for 5 d, and the percentage of the remaining GFP$^+$ fraction were analyzed. Data are representative of four independent experiments. (F) The percentages of the remaining LSK fraction in GFP$^-$ and GFP$^+$ cells after culture were analyzed (*, $P < 0.0001$; $n = 4$). (G) Numbers of CFU-GM, CFU-GEMM, and BFU-E colonies derived from 200 GFP$^-$ and GFP$^+$ cells were analyzed (*, $P < 0.0001$; $n = 4$). (H) Cell cycle status of LSK GFP$^-$ and LSK GFP$^+$ cells from *Evi1*$^{+/GFP}$ mice, analyzed by Hoechst 33342 and pyronin Y staining (*, $P < 0.05$; **, $P < 0.005$; ***, $P < 0.0005$, $n = 3$). Data represent mean ± SD.

Published November 14, 2011

the LSK phenotype (Fig. 3 F), indicating that loss of GFP correlates with phenotypic differentiation. To confirm the differential phenotype of the GFP$^-$ and GFP$^+$ cells after culture reflected their functional status, we compared their ability to form colonies in methylcellulose. GFP$^+$ cells yielded significantly more colonies than GFP$^-$ cells (Fig. 3 G), suggesting that functionally primitive HSCs predominantly reside in the GFP$^+$ fraction. Collectively, these data indicate that in vitro culture of LSK GFP$^+$ cells leads to generation of GFP$^-$ cells that are more differentiated, and lend credence to the use of GFP as a fluorescent sensor for the differentiation state of hematopoietic cells.

To determine the cell-cycle distribution of LSK GFP$^-$ and LSK GFP$^+$ cells, we performed Hoechst 33342 and pyronin Y staining, which revealed that the majority of LSK GFP$^+$ cells were in G_0 phase, whereas a significant proportion of LSK GFP$^-$ cells were actively cycling (Fig. 3 H). These data indicate that, within HSPCs, Evi1 expression represents a functionally distinct population that remains in an undifferentiated and quiescent state.

Evi1 expression marks in vivo long-term multilineage repopulating HSCs in adult BM

Based on the aforementioned data, we hypothesized that Evi1 expression would have the potential to effectively mark long-term multilineage repopulating HSCs. To examine this issue, we performed a CRA, in which 500 purified LSK GFP$^-$ or LSK GFP$^+$ cells were transplanted with 2×10^5 competitor BM cells into lethally irradiated recipients (Fig. S1 A). At 16 wk after transplantation, flow cytometric analysis of donor-derived cells revealed long-term reconstitution in all recipients transplanted with LSK GFP$^+$ cells (Fig. 4 A). Moreover, LSK GFP$^+$ cells displayed multilineage potential with robust contribution to myeloid, B, and T cells in peripheral blood (PB) as well as the LSK

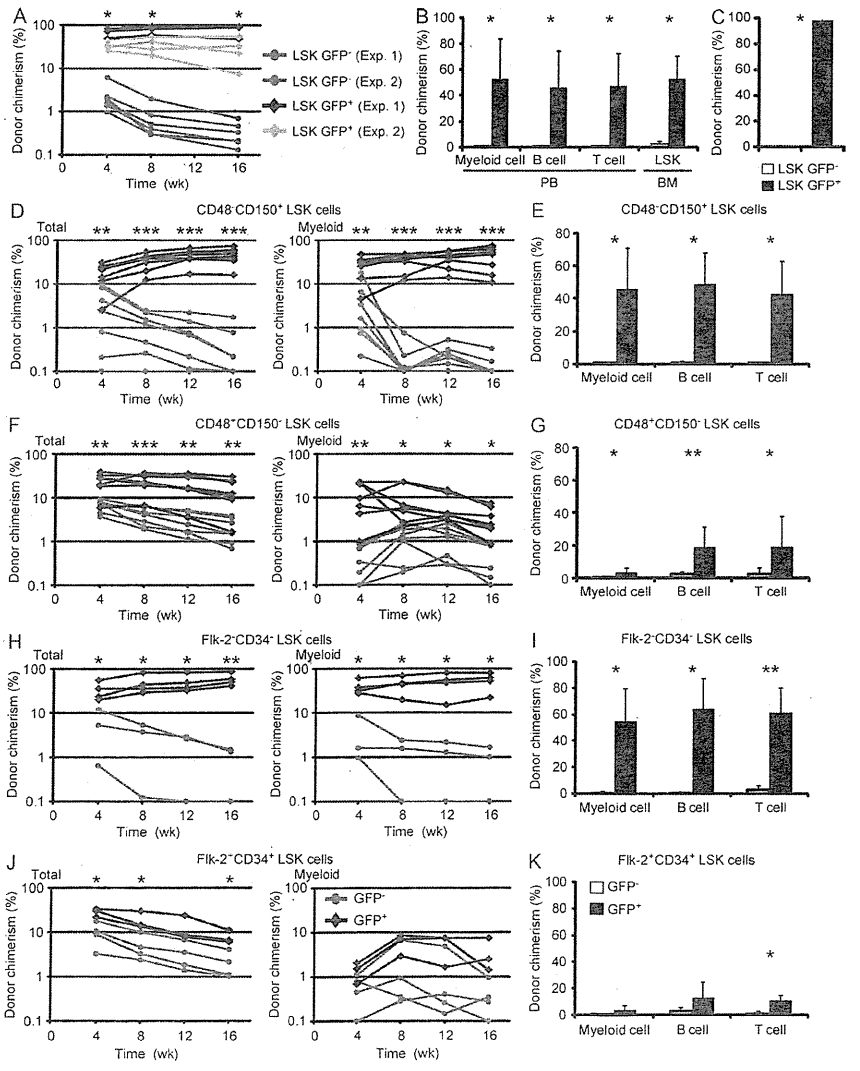

Figure 4. Evi1 expression marks in vivo long-term multilineage repopulating HSCs in adult BM. (A and B) PB donor chimerism in CRAs, in which 500 LSK GFP$^-$ or LSK GFP$^+$ cells sorted from *Evi1*$^{+/GFP}$ mice (Ly5.2) were transplanted into lethally irradiated recipients (Ly5.1) together with 2×10^5 competitor BM cells (Ly5.1 × Ly5.2). (A) Percentages of donor-derived cells (Ly5.2) in PB after transplantation are shown. Each dot indicates an individual recipient mouse (*, $P < 0.005$; $n = 6$–7 from 2 independent experiments). (B) Percentages of donor-derived cells (Ly5.2) in myeloid, B, and T cells of PB and LSK cells of BM 16 wk after transplantation. Recipient mice in experiment 1 were used for the analysis of BM (*, $P < 0.01$; $n = 6$–7 for PB and $n = 3$ for BM). (C) Percentages of donor-derived cells (Ly5.2) in PB of secondary recipient mice (Ly5.1) 16 wk after transplantation. Recipient mice in experiment 1 were used for secondary transplantation (*, $P < 0.0001$, $n = 3$). (D–K) PB donor chimerism in CRAs, in which 100 CD48$^-$ CD150$^+$ LSK GFP$^-$ or CD48$^-$ CD150$^+$ LSK GFP$^+$ cells (D and E; $n = 7$–8), or 500 CD48$^+$ CD150$^-$ LSK GFP$^-$ or CD48$^+$ CD150$^-$ LSK GFP$^+$ cells (F and G; $n = 7$), or 100 Flk-2$^-$ CD34$^-$ LSK GFP$^-$ or Flk-2$^-$ CD34$^-$ LSK GFP$^+$ cells (H and I; $n = 3$–4), or 500 Flk-2$^+$ CD34$^+$ LSK GFP$^-$ or Flk-2$^+$ CD34$^+$ LSK GFP$^+$ cells (J and K; $n = 3$–4) sorted from *Evi1*$^{+/GFP}$ mice (Ly5.1) were transplanted into lethally irradiated recipients (Ly5.2) together with 2×10^5 competitor BM cells (Ly5.2). (D, F, H, and J) Percentages of donor-derived cells (Ly5.1) in total (left) and myeloid cells (right) of PB after transplantation are shown. Each dot indicates an individual recipient mouse (*, $P < 0.05$; **, $P < 0.005$; ***, $P < 0.0005$). (E, G, I, and K) Percentages of donor-derived cells (Ly5.1) in myeloid, B, and T cells of PB 16 wk after transplantation (*, $P < 0.05$; **, $P < 0.005$). Data represent mean ± SD.

Published November 14, 2011

fraction in BM (Fig. 4 B). In contrast, LSK GFP$^-$ cells yielded an almost total inability to generate long-term chimerism (Fig. 4, A and B), which suggests that this population is devoid of self-renewal activity. To confirm the in vivo repopulating capacity of LSK GFP$^+$ cells, we performed secondary transplantation. Similarly, LSK GFP$^+$ cells showed remarkable long-term reconstitution, whereas LSK GFP$^-$ cells consistently failed to produce detectable donor-derived cells (Fig. 4 C), demonstrating that in vivo long-term multilineage repopulating cells are exclusively enriched in the LSK GFP$^+$ fraction in adult BM.

To further refine our analysis designating Evi1 expression as a robust and reliable HSC marker, we compared the repopulating capacity of GFP$^-$ and GFP$^+$ cells within the CD48$^-$ CD150$^+$ LSK fraction, which is enriched for LT-HSCs (Fig. S1 B). Intriguingly, CD48$^-$ CD150$^+$ LSK GFP$^+$ cells exhibited long-term multilineage reconstitution, whereas no engraftment was observed in recipients of CD48$^-$ CD150$^+$ LSK GFP$^-$ cells (Fig. 4, D and E), suggesting that long-term repopulating HSCs predominantly reside in the GFP$^+$ fraction even within the highly subfractionated LT-HSC fraction. We then examined whether Evi1 expression is associated with repopulating capacity in the CD48$^+$ CD150$^-$ LSK fraction, which is enriched for ST-HSCs/MPPs with limited self-renewal activity (Fig. S1 B). Although CD48$^+$ CD150$^-$ LSK GFP$^-$ cells provided only a transient reconstitution, CD48$^+$ CD150$^-$ LSK GFP$^+$ cells showed declining, but sustained engraftment 16 wk after transplantation (Fig. 4 F). In contrast to CD48$^-$ CD150$^+$ LSK GFP$^+$ cells, CD48$^+$ CD150$^-$ LSK GFP$^+$ cells mediated faint myeloid but superior lymphoid reconstitution (Fig. 4, F and G). Although it is controversial whether CD48$^+$ CD150$^-$ LSK cells are transiently reconstituting MPPs/ST-HSCs or lymphoid-biased LT-HSCs with limited long-term engraftment and strong predominance of lymphoid reconstitution (Kiel et al., 2005; Weksberg et al., 2008; Grassinger et al., 2010), Evi1-expressing cells possess higher repopulating capacity within this fraction. When we subfractionated the LSK fraction according to CD34 and Flk-2 expression, and compared the repopulating capacity of GFP$^-$ and GFP$^+$ cells within these subsets (Fig. S1 C), we obtained similar results to the aforementioned findings using SLAM markers (Fig. 4, H–K). These data reveal that, irrespective of the combination of HSC surface markers used, GFP$^+$ cells are the exclusive reservoir of HSC activity, with no reconstitution ability being observed in GFP$^-$ cells within the LT-HSC compartment. Altogether, our results demonstrate that Evi1 expression can further augment the conventional HSC purification strategy, and suggest that Evi1-IRES-GFP knock-in mice allow us to functionally identify HSCs on the ground of self-renewal capacity.

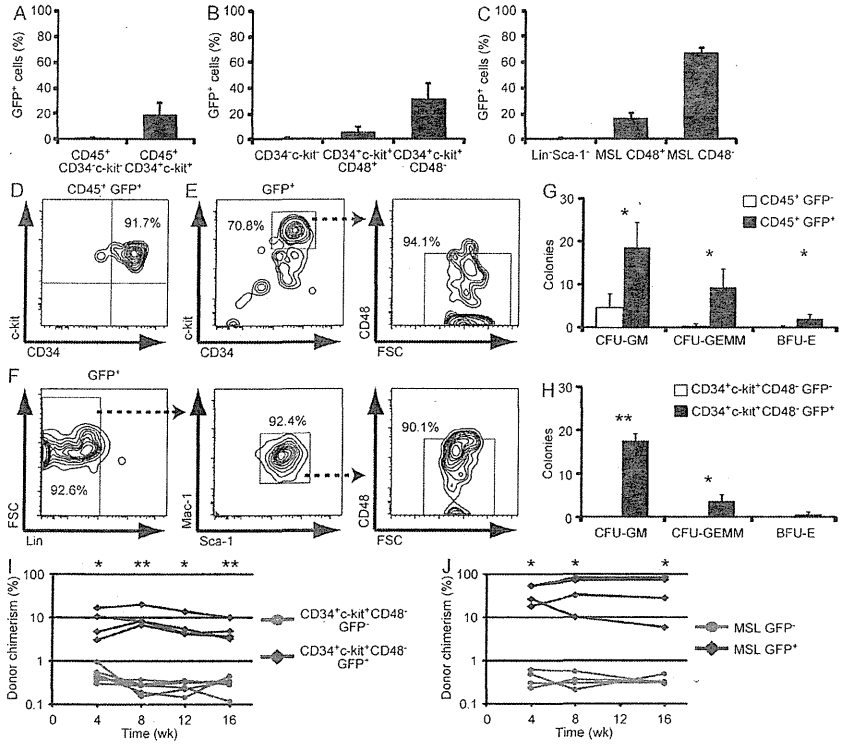

Figure 5. Evi1 expression marks in vivo long-term multilineage repopulating HSCs in embryo. (A–C) Frequency of GFP$^+$ cells in each subpopulation of E10.5 AGM (A; $n = 5$) or E12.5 placenta (B; $n = 3$) or E14.5 FL (C; $n = 5$) from *Evi1*$^{+/GFP}$ embryos. (D–F) FACS analysis of expression of CD34 and c-kit on CD45$^+$ GFP$^+$ cells from E10.5 AGM (D) or CD34, c-kit, and CD48 on GFP$^+$ cells from E12.5 placenta (E) or Lin, Mac-1, Sca-1, and CD48 on GFP$^+$ cells from E14.5 FL (F) in *Evi1*$^{+/GFP}$ embryos. Data are representative of 2 to 10 independent experiments. (G and H) Numbers of CFU-GM, CFU-GEMM, and BFU-E colonies derived from 100 CD45$^+$ GFP$^-$ and CD45$^+$ GFP$^+$ cells sorted from E10.5 AGM (G; $n = 3$), or 100 CD34$^+$ c-kit$^+$ CD48$^-$ GFP$^-$ and CD34$^+$ c-kit$^+$ CD48$^-$ GFP$^+$ cells sorted from E12.5 placenta (H; $n = 3$) in *Evi1*$^{+/GFP}$ embryos (*, $P < 0.05$; **, $P < 0.0005$). (I) PB donor chimerism in CRAs, in which 500 CD34$^+$ c-kit$^+$ CD48$^-$ GFP$^-$ or CD34$^+$ c-kit$^+$ CD48$^-$ GFP$^+$ cells sorted from E12.5 placenta of *Evi1*$^{+/GFP}$ embryos (Ly5.1 × Ly5.2) were transplanted into lethally irradiated recipients (Ly5.2) together with 2 × 10^5 competitor BM cells (Ly5.2). Percentages of donor-derived cells (Ly5.1 × Ly5.2) in PB after transplantation are shown. Each dot indicates an individual recipient mouse (*, $P < 0.05$; **, $P < 0.005$; $n = 4$–6). (J) PB donor chimerism in CRAs, in which 500 MSL GFP$^-$ or MSL GFP$^+$ cells sorted from E14.5 FL of *Evi1*$^{+/GFP}$ embryos (Ly5.2) were transplanted into lethally irradiated recipients (Ly5.1 × Ly5.2) together with 2 × 10^5 competitor BM cells (Ly5.1 × Ly5.2). Percentages of donor-derived cells (Ly5.2) in PB weeks after transplantation are shown. Each dot indicates an individual recipient mouse (*, $P < 0.05$; $n = 4$). Data represent mean ± SD.

Published November 14, 2011

Evi1 expression marks in vivo long-term multilineage repopulating HSCs in embryo

The formation of blood cells begins in the yolk sac of the embryo, and then shifts to the aorta-gonad-mesonephros (AGM) region, and then sequentially to the placenta, fetal liver (FL), and adult BM. There are several major phenotypic and functional differences between fetal and adult HSCs in surface marker profile, cell cycle status, self-renewal potential, gene expression profile, and regulatory mechanism (Mikkola and Orkin, 2006; Orkin and Zon, 2008). Fetal HSCs, in particular, divide rapidly and undergo massive expansion, whereas adult HSCs are mostly quiescent (Bowie et al., 2006). It is known that Evi1 is highly expressed in the yolk sac, paraaortic splanchnopleura, and HSPCs ($CD45^+$ $CD34^+$ $c\text{-}kit^+$) in early embryo (Yuasa et al., 2005). Therefore, we sought to determine whether Evi1 expression can mark fetal HSCs despite their distinct features from adult HSCs, and thus analyzed the expression pattern of GFP in $Evi1^{+/GFP}$ embryos. As expected, GFP expression was highly restricted to HSPCs in the embryonic tissues; $CD45^+$ $CD34^+$ $c\text{-}kit^+$ cells in embryonic day 10.5 (E10.5) AGM, $CD34^+$ $c\text{-}kit^+$ $CD48^-$ cells in E12.5 placenta, and $Mac\text{-}1^+$ $Sca\text{-}1^+$ Lin^- (MSL) $CD48^-$ cells in E14.5 FL (Fig. 5, A–C; Takakura et al., 2000; Kim et al., 2006; McKinney-Freeman et al., 2009). When the distribution of GFP^+ cells in the fetal hematopoietic system was analyzed, most GFP^+ cells exhibited the HSPC-specific marker profile in all embryonic tissues examined (Fig. 5, D–F), indicating the predominant expression of Evi1 in HSPCs during fetal hematopoiesis.

To determine whether Evi1 expression is associated with hematopoietic activity in the embryonic tissues, we performed colony-forming assays in vitro using $CD45^+$ GFP^- and $CD45^+$ GFP^+ cells from E10.5 AGM, and found that $CD45^+$ GFP^+ cells contained almost all colony-forming cells, with few detectable hematopoietic colonies in $CD45^+$ GFP^- cells (Fig. 5 G). In the same manner, within the $CD34^+$ $c\text{-}kit^+$ $CD48^-$ fraction from E12.5 placenta of $Evi1^{+/GFP}$ embryos, colony-forming activity was exclusively present in GFP^+ cells, regardless of colony type (Fig. 5 H). These data suggest that clonogenic hematopoietic progenitors predominantly reside in the Evi1-expressing fraction in fetal hematopoiesis.

To examine whether Evi1 expression would have the potential to effectively mark long-term repopulating HSCs in embryo, we performed a CRA using sorted $CD34^+$ $c\text{-}kit^+$ $CD48^-$ GFP^- and $CD34^+$ $c\text{-}kit^+$ $CD48^-$ GFP^+ cells from E12.5 placenta of $Evi1^{+/GFP}$ embryos (Fig. S2 A). It was obvious that $CD34^+$ $c\text{-}kit^+$ $CD48^-$ GFP^+ cells contributed to the long-term reconstitution of irradiated recipients, whereas donor chimerism was almost undetectable in mice transplanted with $CD34^+$ $c\text{-}kit^+$ $CD48^-$ GFP^- cells (Fig. 5 I), which is in agreement with the results obtained with their adult counterparts. To further assess whether Evi1 expression can enrich long-term repopulating HSCs in embryo, we performed a CRA using purified MSL GFP^- and MSL GFP^+ cells from E14.5 FL (Fig. S2 B). Along with cells in E12.5 placenta, MSL GFP^+ cells gave rise to long-term multilineage reconstitution, whereas no engraftment was observed in recipients of MSL GFP^- cells (Fig. 5 J). These results indicate that fetal HSCs with active *Evi1* transcription exclusively harbor stem cell activity. Collectively, despite the functional differences between fetal and adult HSCs, Evi1 expression marks long-term multilineage repopulating HSCs throughout ontogeny, suggesting a specific relationship between Evi1 expression and HSC self-renewal capacity.

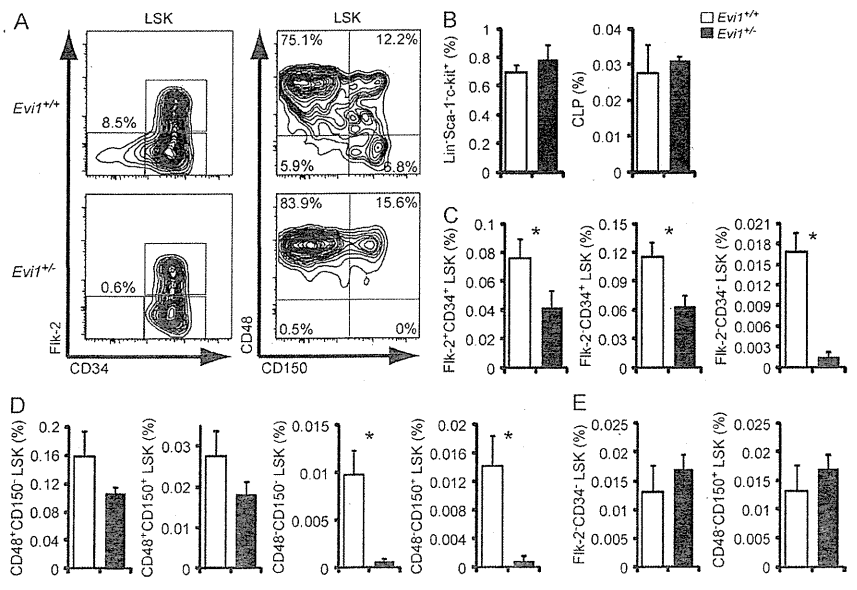

Figure 6. Evi1 heterozygosity leads to an almost complete loss of LT-HSCs in a cell-autonomous manner. (A) FACS analysis of expression of Flk-2 and CD34 or CD48 and CD150 on LSK cells in BM from $Evi1^{+/+}$ and $Evi1^{+/-}$ mice. Data are representative of at least three independent experiments. (B) Frequency of myeloid (Lin^- $Sca\text{-}1^-$ $c\text{-}kit^+$) and lymphoid progenitors (CLPs) in BM from $Evi1^{+/+}$ and $Evi1^{+/-}$ mice ($n = 3$). (C) Frequency of Flk-2^+ $CD34^+$, Flk-2^- $CD34^+$, and Flk-2^- $CD34^-$ subsets within LSK cells in BM from $Evi1^{+/+}$ and $Evi1^{+/-}$ mice (*, $P < 0.0001$; $n = 8$). (D) Frequency of $CD48^+$ $CD150^-$, $CD48^+$ $CD150^+$, $CD48^-$ $CD150^-$, and $CD48^-$ $CD150^+$ subsets within LSK cells in BM from $Evi1^{+/+}$ and $Evi1^{+/-}$ mice (*, $P < 0.01$; $n = 3$). (E) Reciprocal transplantation assay was performed by transplantation of 2×10^5 WT BM cells (Ly5.1) into lethally irradiated $Evi1^{+/+}$ or $Evi1^{+/-}$ mice (Ly5.2). Frequency of Flk-2^- $CD34^-$ LSK or $CD48^-$ $CD150^+$ LSK cells in BM of recipients 16 wk after transplantation is shown ($n = 4$). Data represent mean ± SD.

Published November 14, 2011

JEM

Evi1 heterozygosity leads to an almost complete loss of LT-HSCs in a cell-autonomous manner

The aforementioned observations led us to predict that Evi1 plays a functional role specifically in LT-HSCs. To clarify this issue, we analyzed heterozygous *Evi1* KO mice (*Evi1*$^{+/-}$). We previously showed that heterozygosity of Evi1 leads to decreased numbers of LSK and CD34$^-$ LSK cells, as well as impaired long-term repopulating activity (Goyama et al., 2008). In the current study, although Flk-2$^+$ CD34$^+$ and Flk-2$^-$ CD34$^+$ LSK cells were moderately decreased, Flk-2$^-$ CD34$^-$ LSK cells from *Evi1*$^{+/-}$ mice exhibited a marked reduction in frequency compared with WT controls (Fig. 6, A and C). Likewise, when LSK cells were subdivided according to SLAM markers, we observed substantial decreases in CD48$^-$ CD150$^-$ and CD48$^-$ CD150$^+$ LSK subsets (Fig. 6, A and D). Therefore, the number of each subpopulation within the LSK fraction in *Evi1*$^{+/-}$ mice was declined in proportion to their expression level of Evi1, indicating that Evi1 has a dominating effect on the maintenance of LT-HSCs. In contrast, there were no significant differences in BM cellularity and the frequencies of lymphoid and myeloid progenitors, and mature blood cells between *Evi1*$^{+/+}$ and *Evi1*$^{+/-}$ mice (Fig. 6 B and not depicted), indicating that the differentiation potential to all mature lineages and committed progenitors is normal in *Evi1*$^{+/-}$ mice. Collectively, these observations suggest that Evi1 serves as a specific regulator in the earliest stage of adult hematopoietic development.

To exclude the possibility that a defect of BM microenvironment could be responsible for the observed hematopoietic abnormalities in *Evi1*$^{+/-}$ mice, we performed reciprocal transplantation experiments, in which WT BM cells were transplanted into lethally irradiated *Evi1*$^{+/+}$ or *Evi1*$^{+/-}$ mice. At 16 wk after transplantation, flow cytometric analysis showed no differences in the percentages of Flk-2$^-$ CD34$^-$ LSK or CD48$^-$ CD150$^+$ LSK cells in both groups of recipient mice (Fig. 6 E), demonstrating that the profound loss of LT-HSCs in *Evi1*$^{+/-}$ mice is attributed to cell-intrinsic mechanisms.

Evi1 heterozygosity causes specific abrogation of self-renewal capacity in ST- and LT-HSCs

To further characterize which subpopulation in HSPCs is most dependent on Evi1, we purified CD34$^+$ and Flk-2$^-$ CD34$^-$ LSK cells from *Evi1*$^{+/+}$ and *Evi1*$^{+/-}$ mice and compared their differentiation and self-renewal capacity in vitro and in vivo. First, to assess the effect of Evi1 heterozygosity on the biological functions of ST-HSCs/MPPs, we performed colony-forming assays in vitro using *Evi1*$^{+/+}$ and *Evi1*$^{+/-}$ CD34$^+$ LSK cells, which demonstrated no significant differences in the number and type of colonies (Fig. 7 A). Similarly, we found the capacity of *Evi1*$^{+/-}$ CD34$^+$ LSK cells to form colonies in the spleen 11 d after transplantation (CFU-spleen [CFU-S]) was also equivalent to that of WT littermates (Fig. 7 B), indicating Evi1 is dispensable for the regulation of the differentiation and proliferation capacity in ST-HSCs/MPPs. Moreover, to investigate the self-renewal ability of ST-HSCs/MPPs in vivo, we evaluated the short-term repopulating capacity of purified CD34$^+$ LSK cells using a CRA. At 2 wk after transplantation, we detected comparable frequencies of *Evi1*$^{+/+}$ and *Evi1*$^{+/-}$ CD34$^+$ LSK cell–derived myeloid and B cells (Fig. 7 C), suggesting that heterozygosity of Evi1 does not affect the engraftment and differentiation potential of ST-HSCs/MPPs in vivo. However, at later time points in the experiment, we found a moderate but significant decline in the percentage of donor-derived cells from *Evi1*$^{+/-}$ mice (Fig. 7 D). These data indicate that heterozygosity of Evi1 attenuates the self-renewal capacity of ST-HSCs/MPPs, but is not accompanied by any specific differentiation defects in them.

To assess whether Evi1 is required for the functions of LT-HSCs, we compared the self-renewal and proliferation capacity of *Evi1*$^{+/+}$ and *Evi1*$^{+/-}$ Flk-2$^-$ CD34$^-$ LSK cells when cultured in serum-free medium. *Evi1*$^{+/-}$ Flk-2$^-$ CD34$^-$ LSK cells showed comparable proliferation with WT cells for the first week of culture, but thereafter they exhibited pronouncedly impaired growth (Fig. 7 E). After incubation, a significantly lower proportion of cultured *Evi1*$^{+/-}$ Flk-2$^-$ CD34$^-$ LSK cells remained in the LSK fraction than those from *Evi1*$^{+/+}$ mice (Fig. 7 F). In addition, we observed a prominent reduction of hematopoietic colonies contained in cultured *Evi1*$^{+/-}$ Flk-2$^-$ CD34$^-$ LSK cells (Fig. 7 G). Besides, most of the colonies generated from cultured *Evi1*$^{+/-}$ Flk-2$^-$ CD34$^-$ LSK cells consisted of only CFU-GM. These data indicate that heterozygosity of Evi1 results in accelerated loss of HSPCs, leading to the inefficient expansion of their progeny. To evaluate the colony-forming capacity at the single cell level, *Evi1*$^{+/+}$ and *Evi1*$^{+/-}$ Flk-2$^-$ CD34$^-$ LSK cells were clonally sorted and cultured in serum-free medium. Evi1 heterozygosity diminished the colony-forming efficiency of clone-sorted Flk-2$^-$ CD34$^-$ LSK cells, and single *Evi1*$^{+/-}$ Flk-2$^-$ CD34$^-$ LSK cells generated smaller colonies compared with control cells (Fig. 7 H), which indicates that the disruption of Evi1 gene not only decreases the number of clonogenic HSCs but also impairs the functional output per cell.

To assess the repopulating capacity of *Evi1*$^{+/-}$ LT-HSCs in vivo, we performed a CRA using purified Flk-2$^-$ CD34$^-$ LSK cells from *Evi1*$^{+/+}$ and *Evi1*$^{+/-}$ mice. Notably, *Evi1*$^{+/-}$ Flk-2$^-$ CD34$^-$ LSK cells were almost unable to efficiently repopulate all mature lineages as well as stem and progenitor cells 16 wk after transplantation (Fig. 7, I and J), suggesting that LT-HSC function is critically dependent on Evi1 gene dosage. In a noncompetitive setting, although recipients of *Evi1*$^{+/+}$ and *Evi1*$^{+/-}$ Flk-2$^-$ CD34$^-$ LSK cells had similar survival after transplantation (not depicted), *Evi1*$^{+/-}$ Flk-2$^-$ CD34$^-$ LSK cells showed impaired engraftment (Fig. 7 K), suggesting that *Evi1*$^{+/-}$ HSCs were outcompeted by residual host HSCs. However, some of those recipients exhibited long-term multilineage reconstitution (Fig. 7 K and not depicted), confirming that the multipotent differentiation capacity is not abrogated in *Evi1*$^{+/-}$ mice. To further explore the competitive disadvantage of *Evi1*$^{+/-}$ HSCs, we transplanted WT BM cells into unirradiated *Evi1*$^{+/+}$ or *Evi1*$^{+/-}$ mice.

Published November 14, 2011

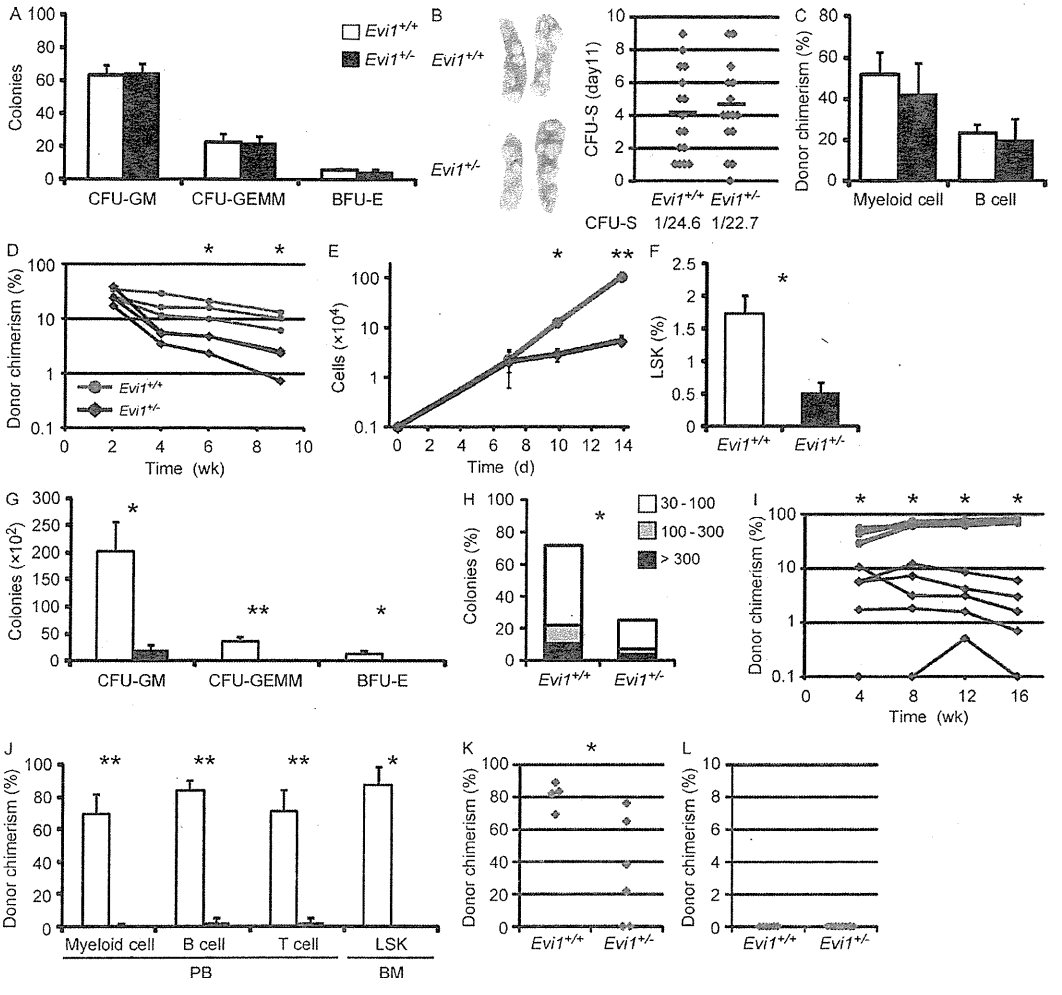

Figure 7. Evi1 heterozygosity causes specific abrogation of self-renewal capacity in ST- and LT-HSCs. (A) Numbers of CFU-GM, CFU-GEMM, and BFU-E colonies derived from 100 sorted *Evi1*$^{+/+}$ and *Evi1*$^{+/-}$ CD34^{+} LSK cells ($n = 3$). (B) Appearance and number of CFU-S colonies in the spleen 11 d after injection of 100 sorted *Evi1*$^{+/+}$ or *Evi1*$^{+/-}$ CD34^{+} LSK cells into lethally irradiated recipients. (left) Representative appearance is shown. (right) Data are shown as a dot plot and each bar represents mean ($n = 15$–16 from 3 independent experiments). (C and D) Short-term in vivo repopulating assay, in which 500 sorted *Evi1*$^{+/+}$ or *Evi1*$^{+/-}$ CD34^{+} LSK cells (Ly5.2) were transplanted into lethally irradiated recipients (Ly5.1) together with 2×10^5 competitor BM cells (Ly5.1). (C) Percentages of donor-derived myeloid and B cells (Ly5.2) in PB 2 wk after transplantation are shown ($n = 3$). (D) Short-term kinetics of the percentages of donor-derived cells (Ly5.2) in PB. Each dot indicates an individual recipient mouse (*, $P < 0.05$; $n = 3$). (E) Proliferation of 1,000 sorted *Evi1*$^{+/+}$ and *Evi1*$^{+/-}$ Flk-2^{-} CD34^{-} LSK cells cultured in serum-free medium supplemented with 20 ng/ml SCF and 20 ng/ml TPO for 14 d (*, $P < 0.01$; ** $P < 0.001$; $n = 3$–4). (F) After 7 d of culture, the percentage of the remaining LSK fraction in cultured *Evi1*$^{+/+}$ and *Evi1*$^{+/-}$ Flk-2^{-} CD34^{-} LSK cells was analyzed (*, $P < 0.005$; $n = 3$). (G) In vitro colony-forming assay was performed to assess the numbers of CFU-GM, CFU-GEMM, and BFU-E colonies after 1,000 *Evi1*$^{+/+}$ and *Evi1*$^{+/-}$ Flk-2^{-} CD34^{-} LSK cells were cultured for 14 d (*, $P < 0.01$; ** $P < 0.001$; $n = 3$–4). (H) Single *Evi1*$^{+/+}$ and *Evi1*$^{+/-}$ Flk-2^{-} CD34^{-} LSK cells were clone-sorted and cultured in serum-free medium. After 14 d of culture, cell numbers in each colony were analyzed. Their relative distribution is shown (*, $P < 0.0001$; $n = 192$ clones from 2 independent experiments). (I–J) Long-term in vivo repopulating assay, in which 200 sorted *Evi1*$^{+/+}$ or *Evi1*$^{+/-}$ Flk-2^{-} CD34^{-} LSK cells (Ly5.2) were transplanted into lethally irradiated recipients (Ly5.1) together with 2×10^5 competitor BM cells (Ly5.1). (I) Percentages of donor-derived cells (Ly5.2) in PB after transplantation are shown. Each dot indicates an individual recipient mouse (*, $P < 0.0001$, $n = 5$–6). (J) Percentages of donor-derived cells (Ly5.2) in myeloid, B, and T cells of PB and LSK cells of BM 16 wk after transplantation (*, $P < 0.001$; ** $P < 0.0001$; $n = 5$–6 for PB and $n = 3$ for BM). (K) Noncompetitive repopulating assay, in which 200 sorted *Evi1*$^{+/+}$ or *Evi1*$^{+/-}$ Flk-2^{-} CD34^{-} LSK cells (Ly5.2) were transplanted into lethally irradiated recipients (Ly5.1) without competitor. Percentages of donor-derived cells (Ly5.2) in PB of recipient mice that survived 12 wk after transplantation are shown (*, $P < 0.05$, $n = 4$–6). (L) Reciprocal transplantation assay was performed by transplantation of 2×10^5 WT BM cells (Ly5.1) into unirradiated *Evi1*$^{+/+}$ or *Evi1*$^{+/-}$ mice (Ly5.2). Percentages of donor-derived cells (Ly5.1) in PB 16 wk after transplantation are shown ($n = 6$–8). Data represent mean ± SD.